Electronic Supplementary Material (ESI) for Organic & Biomolecular Chemistry.

Supplementary Information

A versatile approach towards multivalent saccharide displays on magnetic nanoparticles and phospholipid vesicles

Thomas P. Coxon,[1,2] Thomas W. Fallows,[1,2] Julie E. Gough[3] and Simon J. Webb*[1,2]

[1] School of Chemistry, The University of Manchester, Brunswick Street, Manchester, UK M13 9PL.

[2] Manchester Institute of Biotechnology, The University of Manchester, 131 Princess Street, M1 7DN, Manchester, UK. E-mail: S.Webb@manchester.ac.uk

[3] School of Materials, University of Manchester, MSS Tower, M13 9PL, Manchester, UK.

S.1. Experimental details

Instrumentation: Reversed phase HPLC purification and analysis was performed using an Agilent 110 series system with an Agilent Eclipse XDB-C18 (9.4 x 250 mm) column. Nanoparticle sonication was performed at 20 kHz using a Sonics VCX130PB Ultrasonic processor with a stepped micro tip (3 mm diameter, 136 mm length). Electrospray mass spectrometry was carried out using a Micromass LCT instrument using a Waters 2790 separations module with electrospray ionization and TOF fragment detection. Fluorescence spectra were taken on a Perkin-Elmer LS55 Fluorimeter. UV spectra were taken using a Jasco V-660 spectrometer. QCM-D was performed using a Q-Sense E4 with an Ismatec IPC-N 4 peristaltic pump. NMR spectra were taken in deuterated solvents using either a Brüker 400 Avance spectrometer with broadband probe or a Brüker 500MHz Avance III spectrometer with QCP-F cryoprobe equipped with z-gradients. Chemical shift values are reported in ppm referenced to residual non-deuterated solvent and relative to tetramethylsilane and coupling constants are reported in Hertz (Hz). Multiplicities are reported using the following notations: singlet (s), doublet (d), doublet of doublets (dd), triplet (t) and multiplet (m). Where necessary, COSY, DEPT135 and HMQC experiments were used to aid peak assignment.

Fluorescence images were taken using a Zeiss Axio Imager A1 fluorescence microscope with a Canon Powershot G6 digital camera attached. Confocal microscopy was performed using a Leika TCS SP5. Where necessary, pixel and cell counting analysis was carried out using ImageJ.

Materials: Reagents were purchased from Sigma-Aldrich Co. Ltd., Dorset, UK with the exception of 3,4-dihydroxybenzhydrazide which was purchased from Alfa Aesar, Lancashire, UK and Fluorochem, Derbyshire, UK. All lectins were purchased from Vector Labs with the exception of Wheat Germ Agglutinin which was purchased from Sigma-Aldrich Co. Ltd., Dorset, UK. Magnetite nanoparticles (nanopowder, <50 nm (TEM), ≥98% trace metals basis) were purchased from Sigma-Aldrich Co. Ltd., Dorset, UK. 3,6,9,12-Tetraoxatriacontanehydrazide was synthesised from tetraethylene glycol monooctadecyl ether by a modification of literature procedures; Jones

oxidation,[1] methylation[2] and hydrazinolysis.[3] The intermediates gave the following spectroscopic data. 3,6,9,12-Tetraoxatriacontanoic acid[4]: ^{1}H-NMR (400 MHz, CD_3OD): δ 4.15 (s, 2H, 6), 3.56-3.75 (m, 12H), 3.49 (t, 2H, *J* = 6.9 Hz), 1.59 (m, 2H), 1.31 (m, 30H), 0.92 (t, 3H, *J* = 7.0 Hz). ^{13}C-NMR (101 MHz, $CDCl_3$): δ 178.9, 71.7, 71.4, 70.6 (2C), 70.4, 70.2, 70.1, 69.4, 31.9, 29.7 (10C), 29.6, 29.5, 29.4, 26.0, 22.7, 14.1. Methyl 3,6,9,12-tetraoxatriacontanoate: ^{1}H-NMR (400 MHz, CDCl3): δ 4.11 (s, 2H), 3.69 (s, 3H), 3.48-3.68 (m, 12H), 3.38 (t, 2H, *J* = 6.9 Hz), 1.50 (m, 2H), 1.18 (m, 30H), 0.81 (t, 3H, *J* = 7.0 Hz). ^{13}C-NMR (101 MHz, CD_3OD): δ 177.6, 71.6, 71.0, 70.7 (2C), 70.6 (2C), 70.1, 68.7, 31.9, 29.7 (11C), 29.6, 29.4, 26.1, 22.7, 14.1. 3,6,9,12-Tetraoxatriacontanehydrazide. ^{1}H-NMR (400 MHz, CD_3OD): δ 4.01 (s, 2H), 3.51-3.63 (m, 12H), 3.37 (t, 2H, *J* = 6.9 Hz), 1.50 (m, 2H), 1.18 (m, 30H), 0.81 (t, 3H, *J* = 7.0 Hz). ^{13}C-NMR (101 MHz, CD_3OD): δ 170.6, 71.6, 71.2, 70.6 (2C), 70.5, 70.2, 70.1, 70.0, 31.9, 29.7 (11C), 29.5, 29.4, 26.1, 22.7, 14.1. HRMS for $(C_{26}H_{55}N_2O_5)^+$ expected 475.4105 found 475.4096.

S.2. Magnetic nanoparticle characterisation

General nanoparticle coating procedure: Magnetite nanoparticles (10 mg) were suspended in methanol (5 mL) by probe sonication for 5 minutes. To this suspension was added the desired coating molecule, **X** (**X** = **1a** to **3d**, 0.1 mmol). The sample was sonicated for a further 45 minutes to give **X**-MNP. Remaining coating material was removed by centrifugation, supernatant removal and methanol washing (3 x 10 mL). Finally, the coated nanoparticles were resuspended in milli-Q filtered water (1 mL) and used immediately. For fluorescence microscopy applications, an adaptation of this coating procedure was used, sonicating magnetite nanoparticles (10 mg) in methanol (5 mL) with the desired hydrazone coating molecule along with *N*-(3,4-Dihydroxyphenethyl)-4-(10,15,20-tri-*p*-tolylporphyrin-5-yl)benzamide (total 10 mg, ratio of 9:1 hydrazone:porphyrin).

The extent of coating was determined by elemental analysis on commercial MNPs coated with **3a** (Glc-catechol), which gave measured values of C 0.88 %, H < 0.3 % and N < 0.3 %. A coating efficiency of (1.9 ± 1.1) % wt/wt of **3a** on the MNPs gives calculated values of C (0.88 ± 0.50) %, H (0.10 ± 0.06) % and N (0.15 ± 0.09) %.

Dynamic Light Scattering (DLS): DLS was carried out using a Malvern Zeta-sizer Nano S.

(1) Magnetic nanoparticles (MNPs). Uncoated commercial MNPs obtained from Sigma-Aldrich (specifications: nanopowder, <50 nm (TEM), ≥98% trace metals basis) were diluted to a concentration of 6×10^{-7} mg/mL in deionized water to minimize aggregation. Commercial magnetic nanoparticles (MNPs) coated with **3b** (GlcNAc-catechol conjugate) were also analysed at the same concentration. For each sample, three runs of 15 measurements were recorded. The raw scattering data was converted into number distribution charts by entering the refractive index of magnetite (2.42). The DLS data confirmed that uncoated commercial MNPs particles were <50 nm in diameter, and the data fitted well to the sum of two Gaussian populations centred on 36 nm and

55 nm (Figure S2.1). The MNPs coated with **3b** were found to fit a single Gaussian population with a size of 30 nm. A bimodal distribution could not be unambiguously determined from these data, which we believe is either due to the effect of the coating on solvation or simply the error inherent in DLS measurements on different samples.

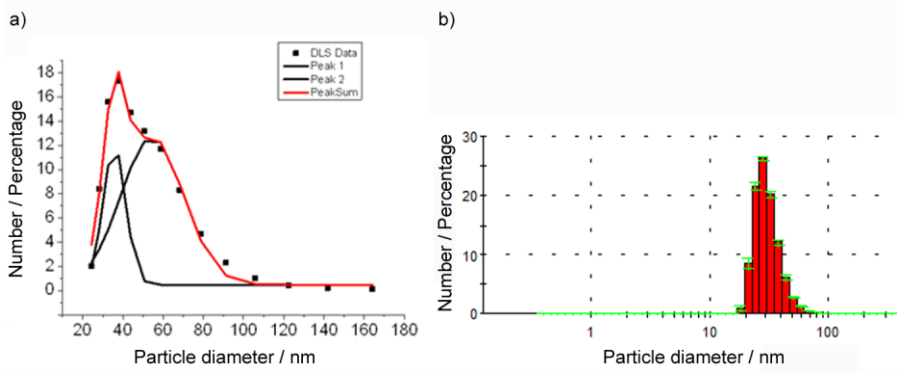

Figure S2.1: DLS data obtained for (a) uncoated commercial MNPs, fitted to two Gaussian populations (at 36 nm and 55 nm). (b) GlcNAc-coated (**3b**) commercial MNPs, fitted to a single Gaussian population (at 30 nm).

(2) Sonicated vesicles. Probe sonicated DMPC vesicles were diluted in HEPES buffer (1 mM). For each sample, three runs of 15 measurements were recorded. The raw scattering data was converted into number distribution charts by entering the refractive index for protein (1.45). The DLS data confirmed that sonicated vesicles were <50 nm in diameter, with a number average of 28 ± 2 nm.

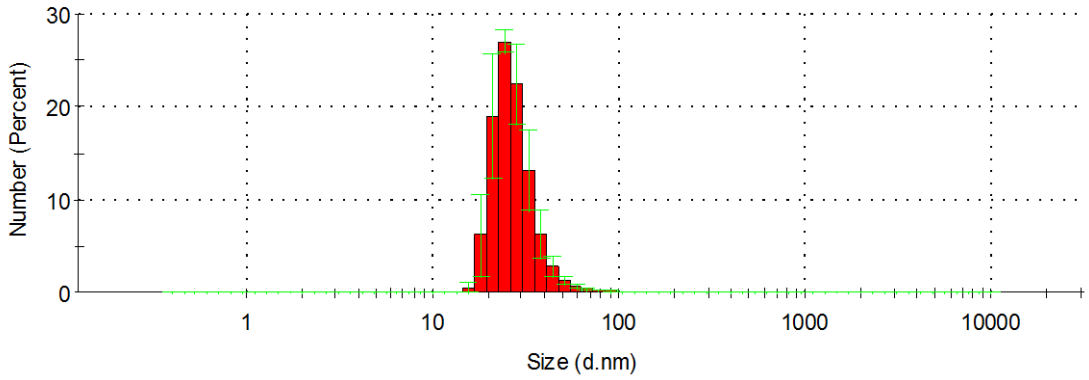

Figure S2.2: DLS data obtained for probe sonicated DMPC vesicles were diluted in HEPES buffer (1 mM), fitted to a single Gaussian population at 28 nm.

Transmission electron microscopy (TEM): TEM was performed using a Philips CM20 operating at 200 keV on both uncoated commercial magnetic nanoparticles and commercial magnetic nanoparticles coated with **3b**. The TEM images of the uncoated MNPs confirm the size distribution obtained by DLS, with a variety of sizes observed. The TEM of the MNPs coated with **3b** show an unchanged appearance and size distribution (Fig. S2.3). The coating of **3b** on the surface may only be ca. 1.3 nm (one molecule) thick and this thin organic layer may not be visible under the TEM conditions used to image the Fe-O core.

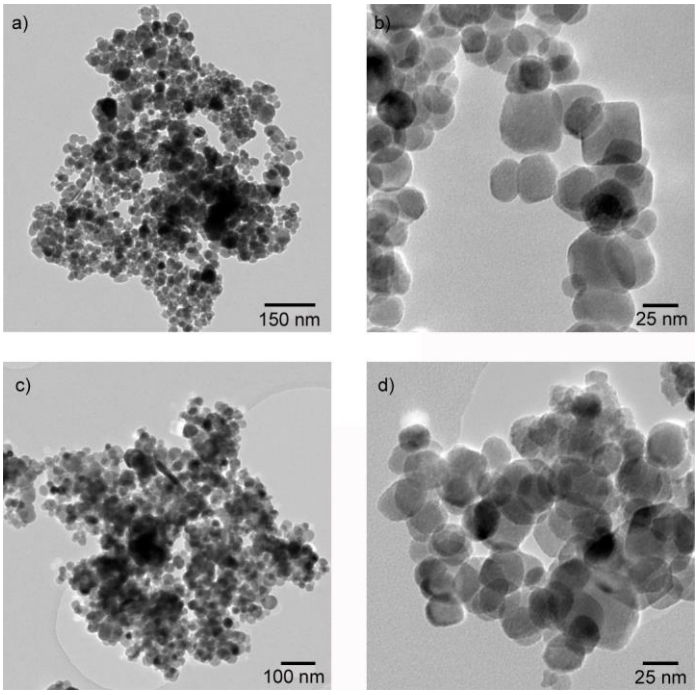

Figure S2.3: TEM images of (a) commercial magnetic nanoparticles (sourced from Sigma-Aldrich), scale bar 100 nm. (b) Commercial magnetic nanoparticles (sourced from Sigma-Aldrich), scale bar 25 nm. (c) Commercial magnetic nanoparticles (sourced from Sigma-Aldrich) coated with **3b**, scale bar 150 nm. (d) Commercial magnetic nanoparticles (sourced from Sigma-Aldrich) coated with **3b**, scale bar 25 nm.

S.3. Hydrolytic stability assessment

A series of buffers were made up at different pD values using sodium phosphate and deuterated trifluoroacetic acid in deuterium oxide, with a total salt concentration of 10 mM. **1a** (10 mg) was then dissolved in these buffers and incubated at room temperature (approx. 25° C) over 23 days. Hydrolysis was monitored over time by taking ^{1}H-NMR spectra at intervals.

Buffer calculations are considerably more complicated for deuterated buffers, because the pK_a values are influenced by the isotope effect.[5] Instead, sodium phosphate and deuterated trifluoroacetic acid were titrated while monitoring pH with a probe. A titration curve (Figure 3.1) was then established, taking into account the correction factor required to calculate pD from probe-measured pH values (pD = measured pH + 0.41).[6] From this, it was possible to determine the relative amounts of the two components that would be required to give a buffer of a certain pH level.

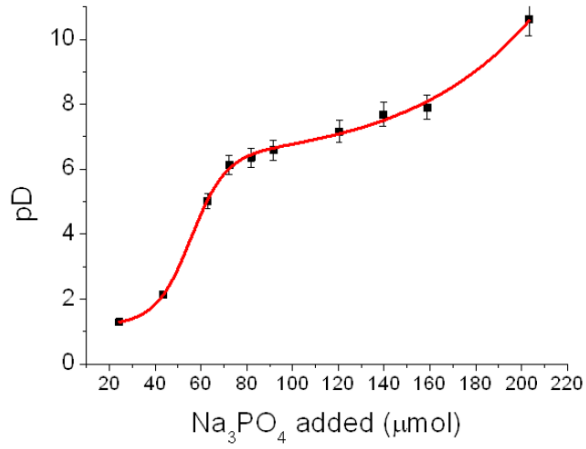

Figure S3.1: Titration curve obtained from the addition of sodium phosphate, dissolved in deuterium oxide, to d_4-trifluoroacetic acid (25 μL), also in deuterium oxide.

Using this titration curve, a series of deuterated buffers were made up in deuterium oxide at a variety of pH levels from 1 to 10. **1a** (10 mg) was then dissolved in each of these and ^{1}H-NMR spectra were taken at intervals. At each pD, degradation appeared to be pseudo first order, with an exponential decay curve fitting well to the data, as shown in Figure S3.2.

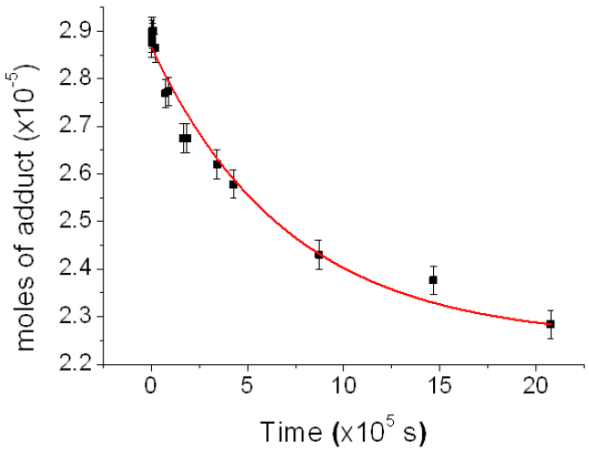

Figure S3.2: Plot of moles of adduct against time, for **1a** (10 mg) dissolved in deuterated buffer (sodium phosphate and d_4-trifluoroacetic acid in deuterium oxide) at pD 7.34. The number of moles of adduct was determined from the integration of anomeric peaks in ^{1}H-NMR spectra. Fitted to the data is an exponential decay curve.

From these decay curves, observed rate constants could be obtained for each pD level, using Equation 3.1.

$$[\boldsymbol{X}] = [\boldsymbol{X}]_{\boldsymbol{0}}\boldsymbol{e}^{-\boldsymbol{k}_{\boldsymbol{obs}}\boldsymbol{t}} \qquad \textbf{Equation 3.1}$$

The good fit of these exponential decay curves suggests that the hydrolysis process was first order with respect to the adduct concentration. If the degradation was also first order with respect to proton concentration, plotting k_{obs} against $[H^+]$ would give a linear fit. This was not the case though (Figure S3.3). Instead, the data fitted better to a curve of the form $k_{obs} = a[H^+]^b$, where *a* and *b* are constants.

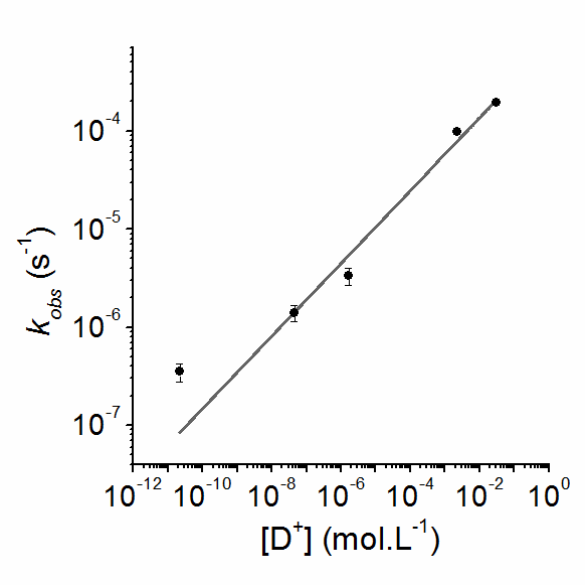

Figure S3.3: Plot of observed rate constant values against proton concentration with a non-linear curve fit of the form $k_{obs} = a[H^+]^b$.

In this case, the coefficient, *a*, would be the rate constant and the power, *b*, would be the rate order with respect to [H^+]. This plot, therefore, actually suggests that hydrolytic rate is around 0.37 order with respect to [H^+]. This means that the observed hydrolysis must have a complex mechanism, possibly proceeding *via* more than one pathway with varying pH dependency.

This fits with the complex, multi-step hydrolysis mechanism put forward by Kalia *et al.*,[7] which contains multiple steps that would be affected by pH and it is therefore unsurprising that the reaction rate has a fractional order with respect to proton concentration.

Bringing together the data from this analysis, Equation 3.2 can be obtained as the overall rate equation.

$$\boldsymbol{r = 5 \times 10^{-4}[H^+]^{0.37}[adduct]} \qquad \textbf{Equation 3.2}$$

S.4. Magnetite nanoparticle coating stability assay

Magnetite nanoparticles were coated with **4** or **5** using the general procedure outlined in S.1. These nanoparticles (2 mg) were then suspended in PBS, MOPS, DMEM buffer (20 mL, pH 7.4) and phosphate buffer 20 mL, pH 6.5 to give a concentration of 0.1 mg/mL. From this suspension, aliquots (2 mL) were taken at different time points, with homogeneity ensured each time by probe sonication of the sample for 5 minutes before removing the aliquot. The nanoparticles were sedimented using a permanent magnet (0.51 T). The supernatant fluorescence was then measured at 520 nm, with increases in fluorescence being the result of unbound **4** or **5** (Figure S4.1). The rate constants of the loss of these coating molecules were obtained from fitting exponential decay curves.

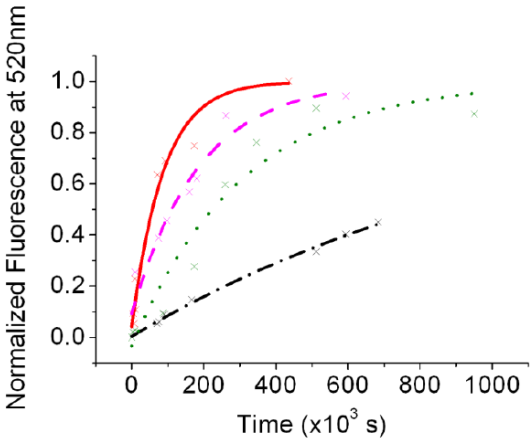

Figure S4.1: Plot of fluorescence against time for the supernatant of a suspension of magnetite nanoparticles coated with **4** assessed in PBS (solid line), MOPS (dashed line) and DMEM (dotted line), all at pH 7.4, and in phosphate buffer at pH 6.5 (dot-dash line).

S.5. Quartz crystal microgravimetry with dissipation

Stock solutions: All solutions were made up in 2-[4-(2-hydroxyethyl)piperazin-1-yl]ethanesulfonic acid (HEPES) buffer (10 mM, 150 mM NaCl, 2 mM $CaCl_2$, pH 7.4). All solutions of lectins, vesicles and MNPs used in the QCM-D had the same mass concentration of 0.1 mg mL^{-1} in HEPES (0.1 mg mL^{-1} lipid for vesicles). Solutions were introduced to the QCM sensor *via* tubing incorporating a peristaltic pump operating at a constant flow rate of 50 μL per minute. During measurements the temperature was controlled at 25°C.

Experimental procedure: QCM-D without lipid bilayer was performed using gold-coated QCM sensors. These sensors were functionalized by incubating for 16 h in a solution of 3-mercaptopropionic acid in ethanol (5 mL, 10 mM). HEPES buffer was flowed over the sensor until a stable baseline was established. Then a solution of the appropriate lectin was flowed over the QCM-D, until no further lectin deposition was observed. HEPES buffer was flowed through again to remove any loose material then control magnetite nanoparticles, coated with polyvinylpyrrolidone, were flowed through. This was followed by more HEPES buffer then MNPs coated with a mismatched saccharide. Finally, MNPs with a matched saccharide coated were flowed through.

QCM-D with lipid bilayer was performed using silica-coated QCM sensors. A lipid film was first produced with a total of 20 μmol lipid, by adding DMPC (14 mg, 95 % mol/mol) to the appropriate glycolipid **2b** or **2c** (5 % mol/mol) in chloroform and then removing the solvent by rotary evaporation. After adding HEPES buffer the lipid film was resuspended by vortexing and the resulting multilamellar vesicles were probe sonicated for 20 mins to form uniform vesicles of approximately 50 nm diameter, as reported by Seantier *et al*.[8] A suspension of these DMPC vesicles was then flowed through the QCM-D. Following deposition and subsequent rupture of these vesicles, HEPES buffer was flowed through until a stable frequency was attained. Then a solution of the appropriate lectin was flowed over the QCM-D, until no further lectin deposition was

observed. HEPES buffer was flowed through again to remove any loose material then control magnetite nanoparticles, coated with polyvinylpyrrolidone, were flowed through. This was followed by more HEPES buffer then MNPs coated with a mismatched saccharide. Finally, MNPs with a matched saccharide coated were flowed through.

In addition to the experiments reported, **1c**-MNP was flowed over a silica coated sensor on which had previous ly been deposited a **2c**-funtionalized DMPC phospholipid bilayer (Figure S5.1).

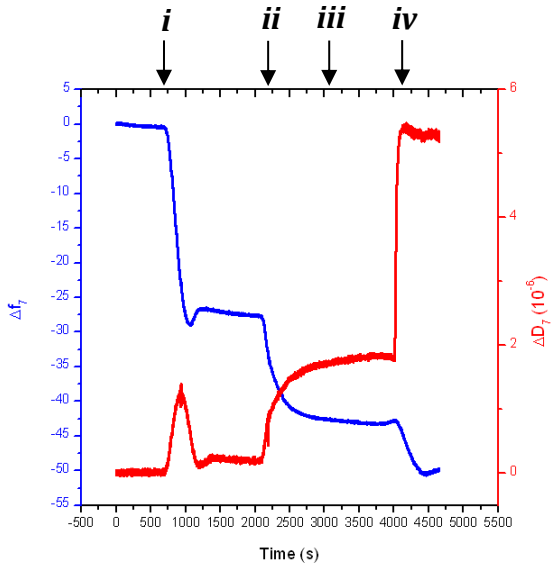

Figure S5.1: Quartz Crystal Microbalance with Dissipation (QCM-D) traces. Frequency over time is shown in blue while dissipation is shown in red. The binding of **1c**-MNP to *Erythrina crytagalli* lectin required the prior deposition of a phospholipid bilayer functionalised with glycolipid **2c**. Arrows (i), (ii), (iii), and (iv) on the trace indicate functionalised vesicles, lectins, mismatched nanoparticles or matched nanoparticles interacting with the chip.

S.6. UV lectin binding assay

Calibration curves were created, measuring absorbance at 280 nm and 25°C for lectin solutions of known concentration dissolved in HEPES buffer (10 mM, 150 mM NaCl, 2 mM $CaCl_2$, pH 7.4). In each case, a linear relationship between absorbance and concentration was observed.

Saccharide coated nanoparticles (10 mg/mL, from Sigma Aldrich) were then added in aliquots (10 µL) to an 8.2 µmol/L lectin solution. After each addition, the solution was stirred for 10 minutes before applying a permanent magnet (0.51 T) to sediment the nanoparticles, along with any bound lectin before measuring absorbance of the supernatant at 280 nm. The change in absorbance at each point was assumed to be due to the concentration decrease caused by binding of lectin to the saccharide-functionalised nanoparticles. The nanoparticle concentration could then be plotted against the percentage of bound lectin and fit to a sigmoidal isotherm using the Hill equation (Figure S6.1).

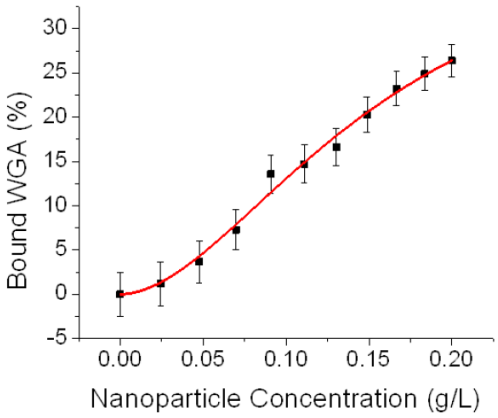

Figure S6.1: Plot of percentage bound wheat germ agglutinin (calculated from UV absorbance at 280 nm after magnetic sedimentation, using a calibration curve) against magnetite nanoparticle concentration, following addition of nanoparticles, coated with resorcinol-based GlcNAc adduct, **1b**, to a lectin solution.

Control experiments were performed using the same lectins and nanoparticles with a mismatched saccharide coating. These showed only slight fluctuations in absorbance at 280 nm, proving that the

consistent decreases observed with matched nanoparticles were due to specific binding between the lectin and the saccharide coating.

S.7. Cell-nanoparticle interaction studies

Cell culture: 3T3 cells were cultured in 25 mL culture flasks, using Dulbecco's Modified Eagle Media (DMEM) with added fetal bovine serum (10% v/v) and antibiotics (1% v/v penicillin and streptomycin) and storing at 37°C. Cells were cultured at confluence, using trypsin to detach the cells before splitting into fresh culture flasks at a dilution of 1 in 5.

Fluorescent staining of cell membranes: Cell membranes were stained using PKH67 (Green) from Sigma Aldrich, following the provided protocol. Briefly, cells were detached using trypsin and washed repeatedly using serum-free DMEM. Cells were then suspended in the provided buffer, Diluent C, before adding to a solution of PKH67 fluorescent marker. Cells were incubated in this solution for 5 minutes before adding DMEM (10 mL) with added fetal bovine serum (10% v/v). Cells were washed repeatedly with DMEM to remove any remaining dye, before seeding onto a well plate or culture flask at the desired concentration.

Cell microscopy experiments: Cells were seeded onto glass cover slips inside a 24-well plate (1 mL/well) at 40,000 cells per mL and incubated for 24 h. Suspensions of **X**-MNP in milli-Q filtered water were then added to give the desired nanoparticle concentration (0.01 mg/well or 0.1 mg/well for pixel counting experiments) and incubated for a further 3 h. For confocal microscopy, cover slips were washed with PBS buffer and then with acid (0.1 M glycine buffer with 0.15 M NaCl at pH3). They were washed thoroughly once more with PBS buffer and fixed with paraformaldehyde before mounting onto a microscope slide using ProLong® Gold with DAPI (from Life Technologies). The mounting agent was allowed to cure for 18 h at room temperature before imaging. Experiments were repeated three times in triplicate.

Study of cell-nanoparticle interaction by microscopy: 1b-MNPs were incubated with 3T3 cells for 3 h at 37°C. Bright field microscopy showed that almost all observable nanoparticles were interacting with the cells in some way (Figure S7.1). Control experiments were done with uncoated nanoparticles.

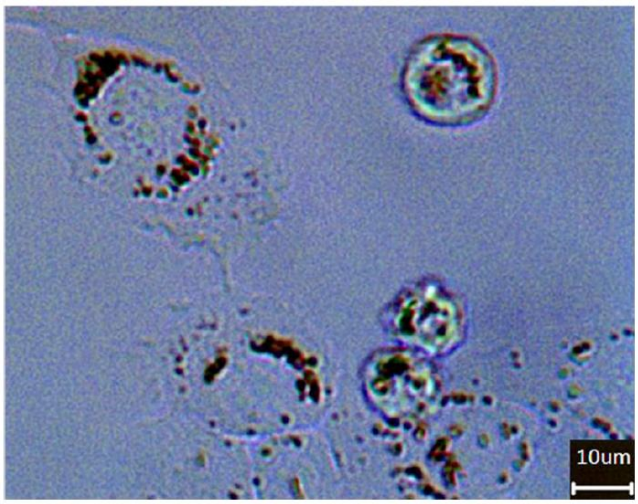

Figure S7.1: Bright field optical microscopy of 3T3 fibroblasts after 3 h incubation with **1b**-MNP.

Competitive interactions between free GlcNAc and 3b-coated MNPs for 3T3 fibroblasts.

3T3 Cells were seeded onto glass cover slips inside a 24-well plate (1 mL/well) at 40,000 cells per mL and incubated for 24 h. *N*-Acetylglucosamine (100 μL, 0.1 mg/mL in water, 45 nmol per well) was added to the wells and incubated (2 h). Suspensions of **3b**-MNP (100 μL, 0.01 mg/mL, 0.001 mg/well, 9:1 **3b**:**6**) were added to the well and incubated (2 h).

The cover slips were washed with PBS buffer then fixed with paraformaldehyde. They were washed thoroughly again with PBS buffer then mounted onto a microscope slide using ProLong® Gold with DAPI (from Life Technologies). The mounting agent was allowed to cure for 18 h at room temperature before imaging.

The concentration of **3b** on the MNP was calculated according to the estimated coating efficiency

of **3a** on MNPS, of 1.9 % wt/wt (see S2 above). This would correspond to 0.19 μg/mL (0.19 mg/L) of **3b**, or 0.5 μmol/L.

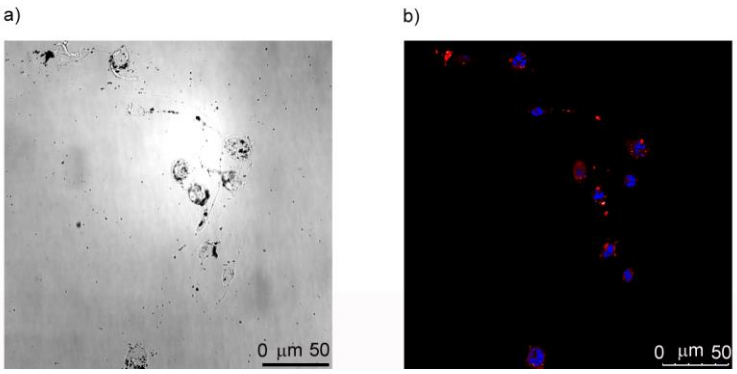

Figure S7.2: 3T3 fibroblasts after incubation with first GlcNAc (2 h) and then **3b**-MNP (2 h). (a) Bright field optical microscopy (b) Overlaid fluorescence microscopy images showing nuclei stained with DAPI (blue) and magnetite nanoparticles (red) coated with **3b** (GlcNac/catechol) and **6** (porphyrin/catechol).

S.8. Spectroscopic data for novel compounds

3,5-Dihydroxy-N'-(1-deoxyglucopyranos-1-yl)-benzohydrazide **1a**

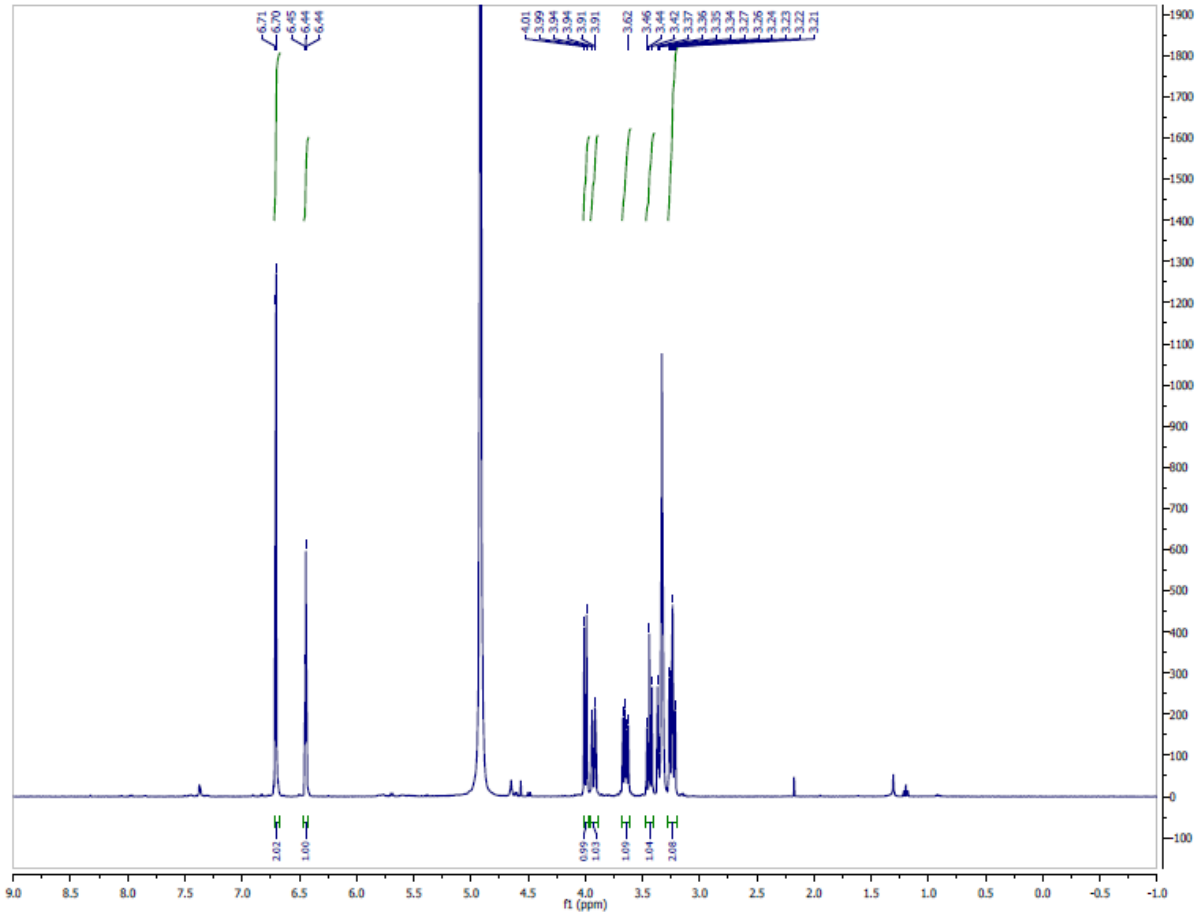

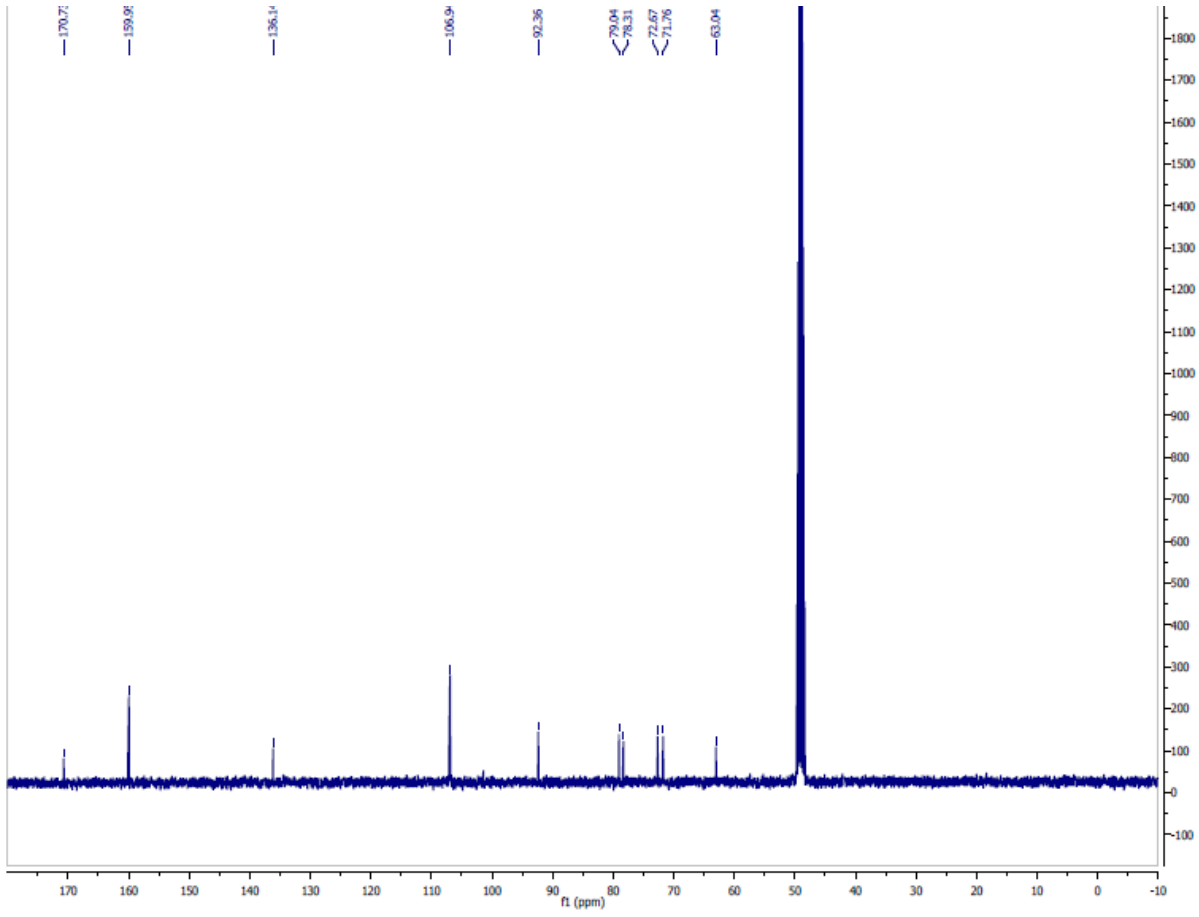

3,5-Dihydroxy-N’-(1,2-dideoxy-2-(acetylamino)-glucopyranos-1-yl)-benzohydrazide **1b**

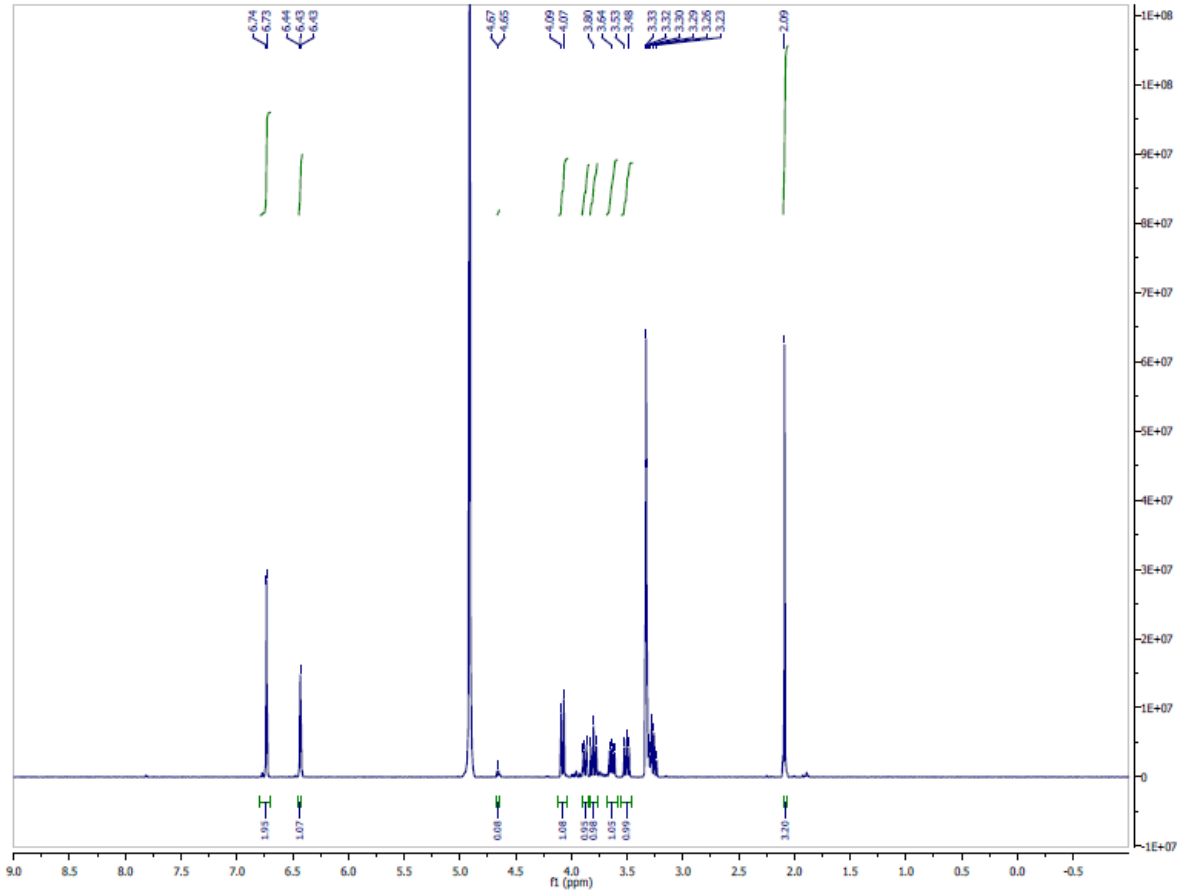

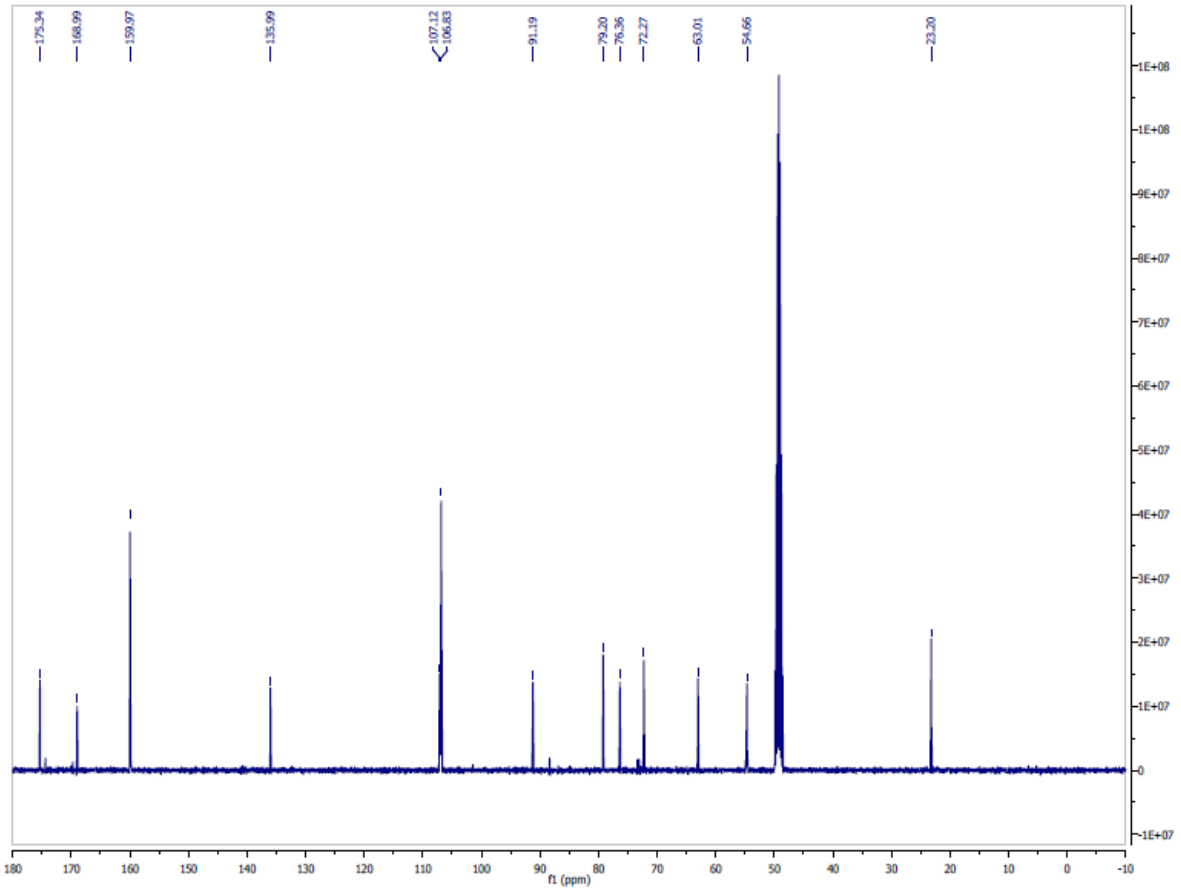

3,5-Dihydroxy-N’-(4-O-(β-galactosyl)-1-deoxyglucopyranos-1-yl)-benzohydrazide **1c**

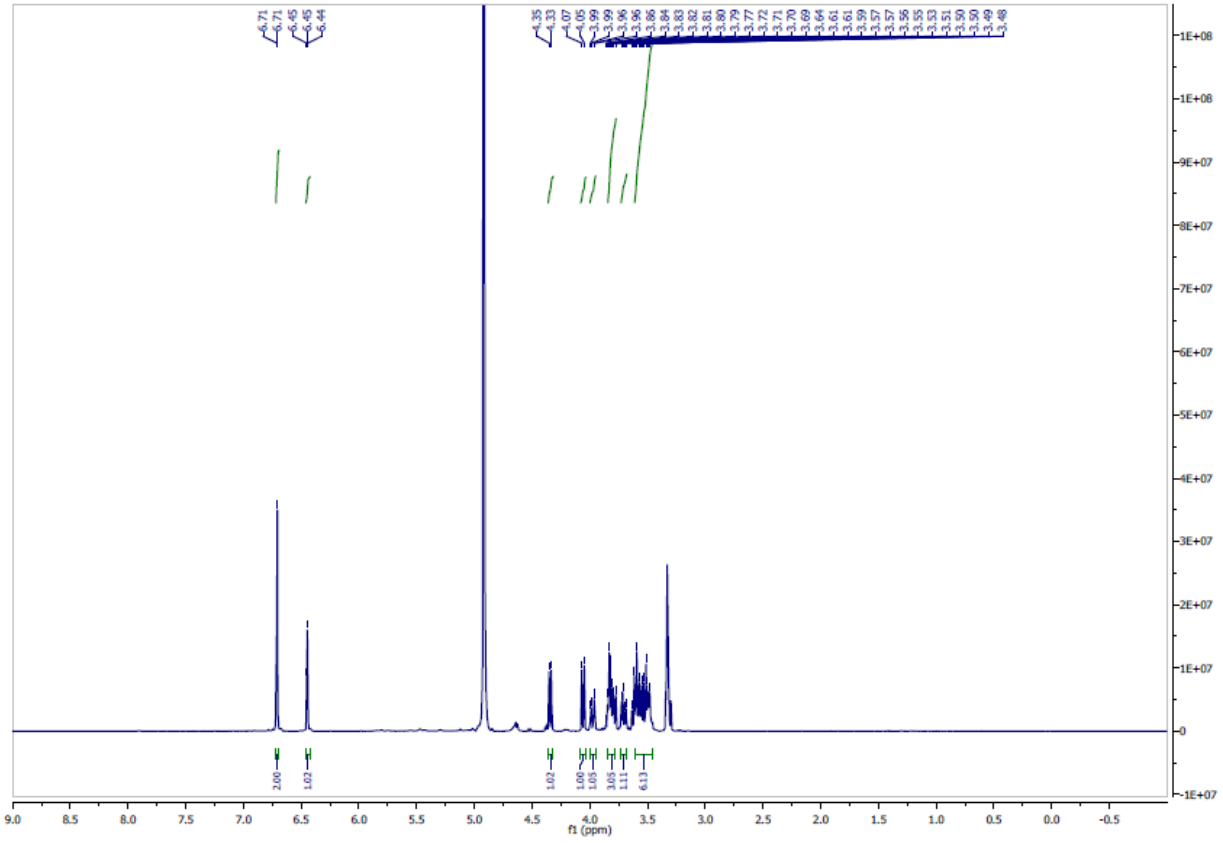

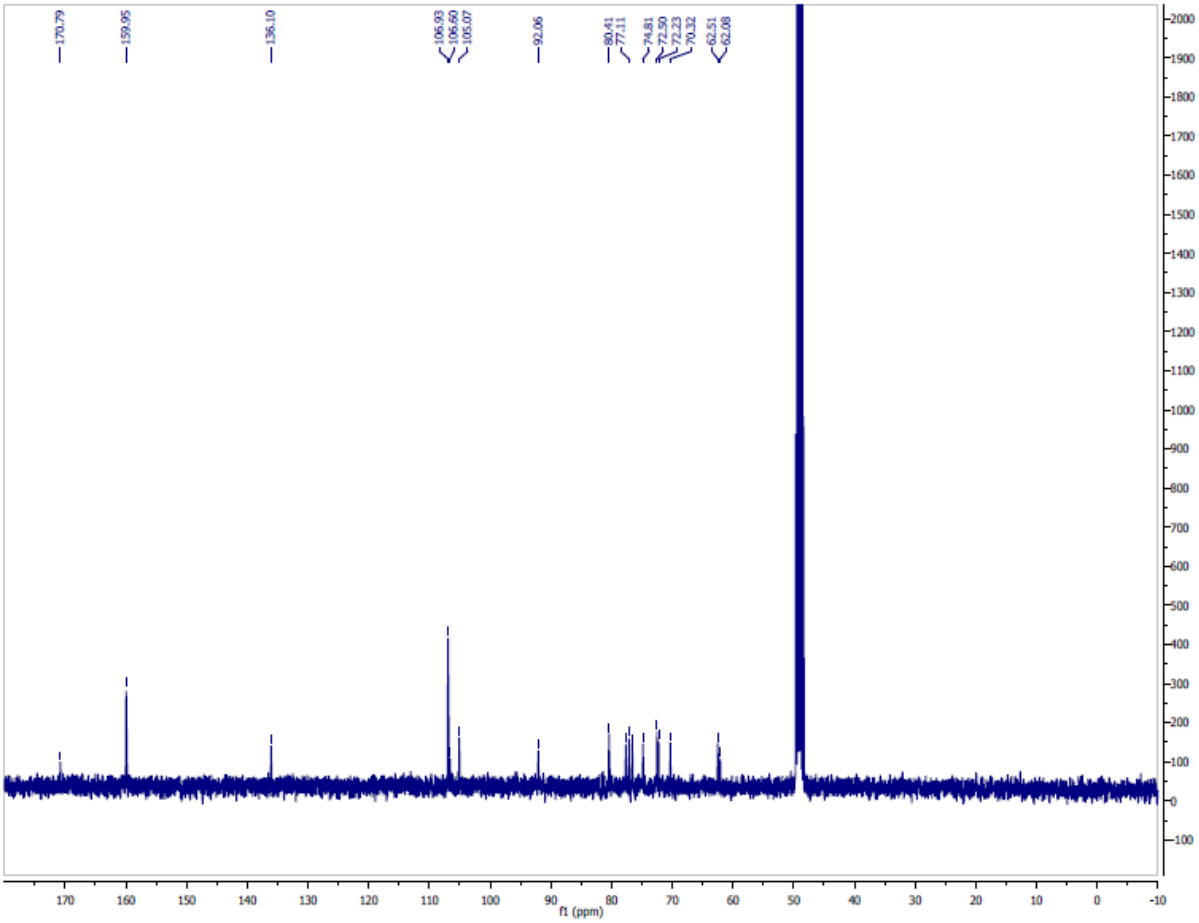

3,5-Dihydroxy-N’-(1-deoxy-4-O-(3-O-(N-acetyl-α-neuraminosyl)-β-galactopyranosyl)glucopyranos-1-yl)-benzohydrazide **1d**

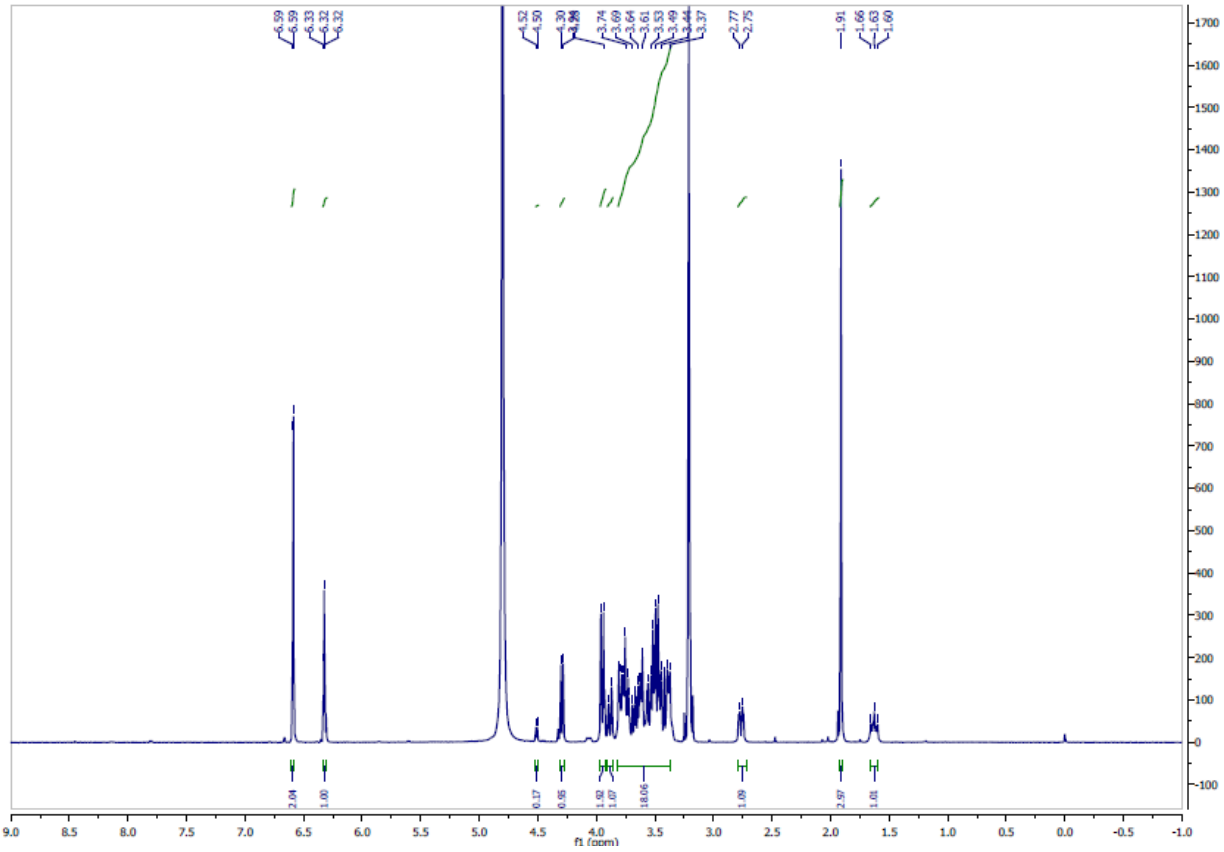

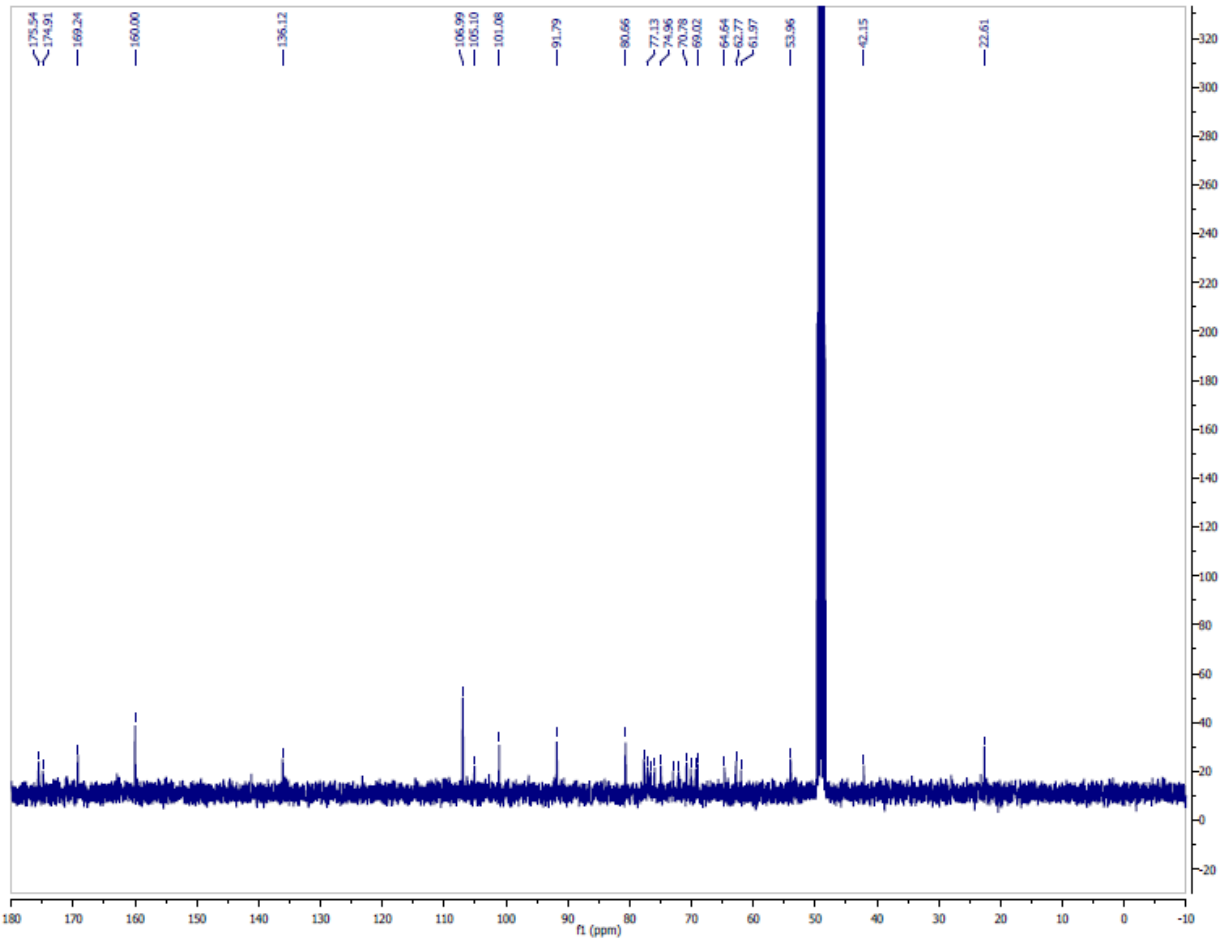

N’-(1-Deoxyglucopyranos-1-yl)-3,6,9,12-tetraoxatriacontanehydrazide **2a**

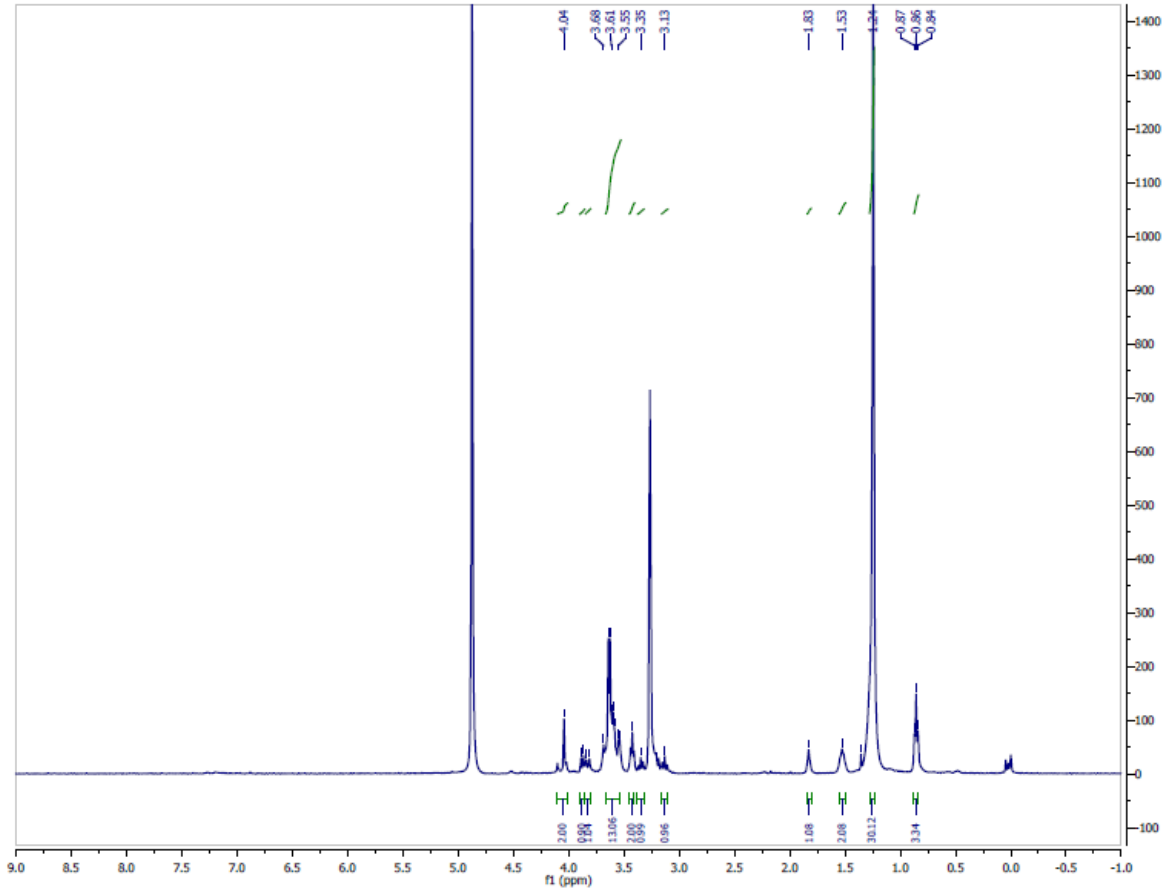

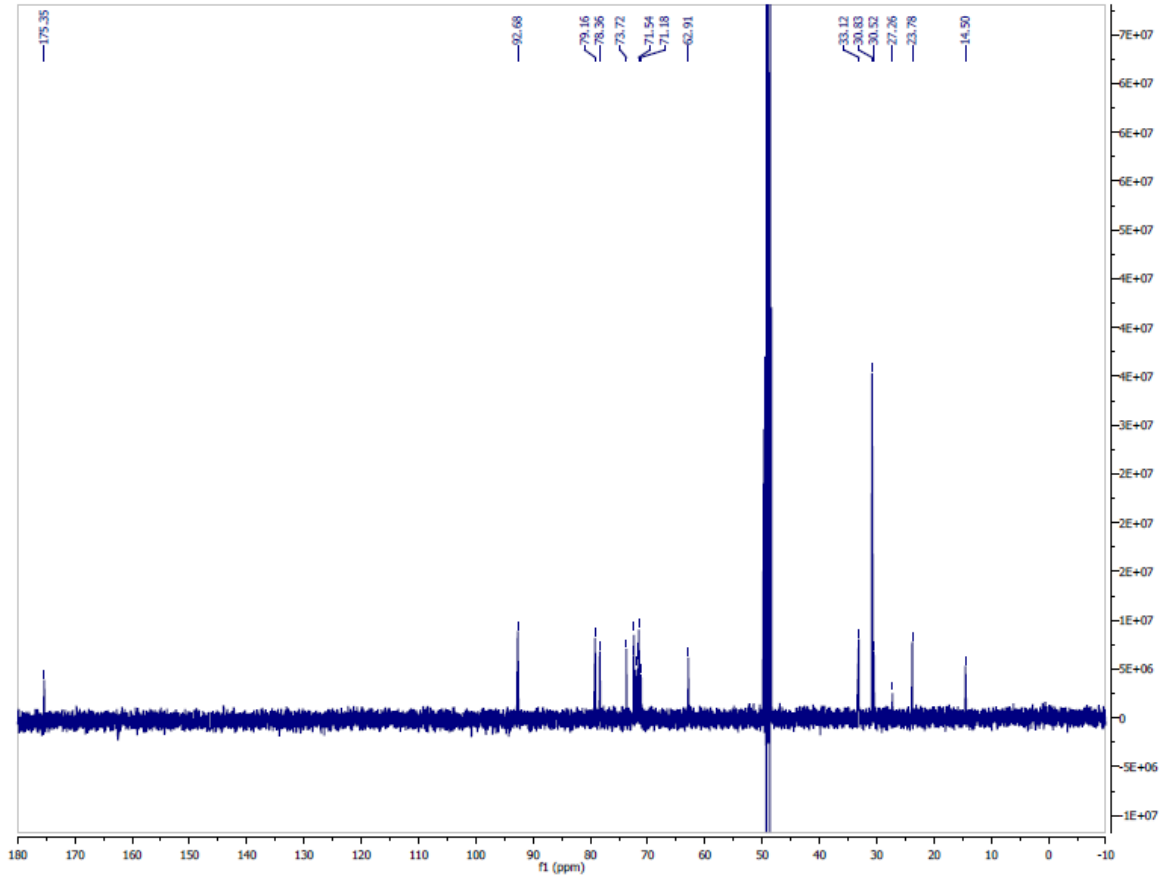

N’-(1,2-Dideoxy-2-(acetylamino)-glucopyranos-1-yl)-3,6,9,12-tetraoxatriacontanehydrazide **2b**

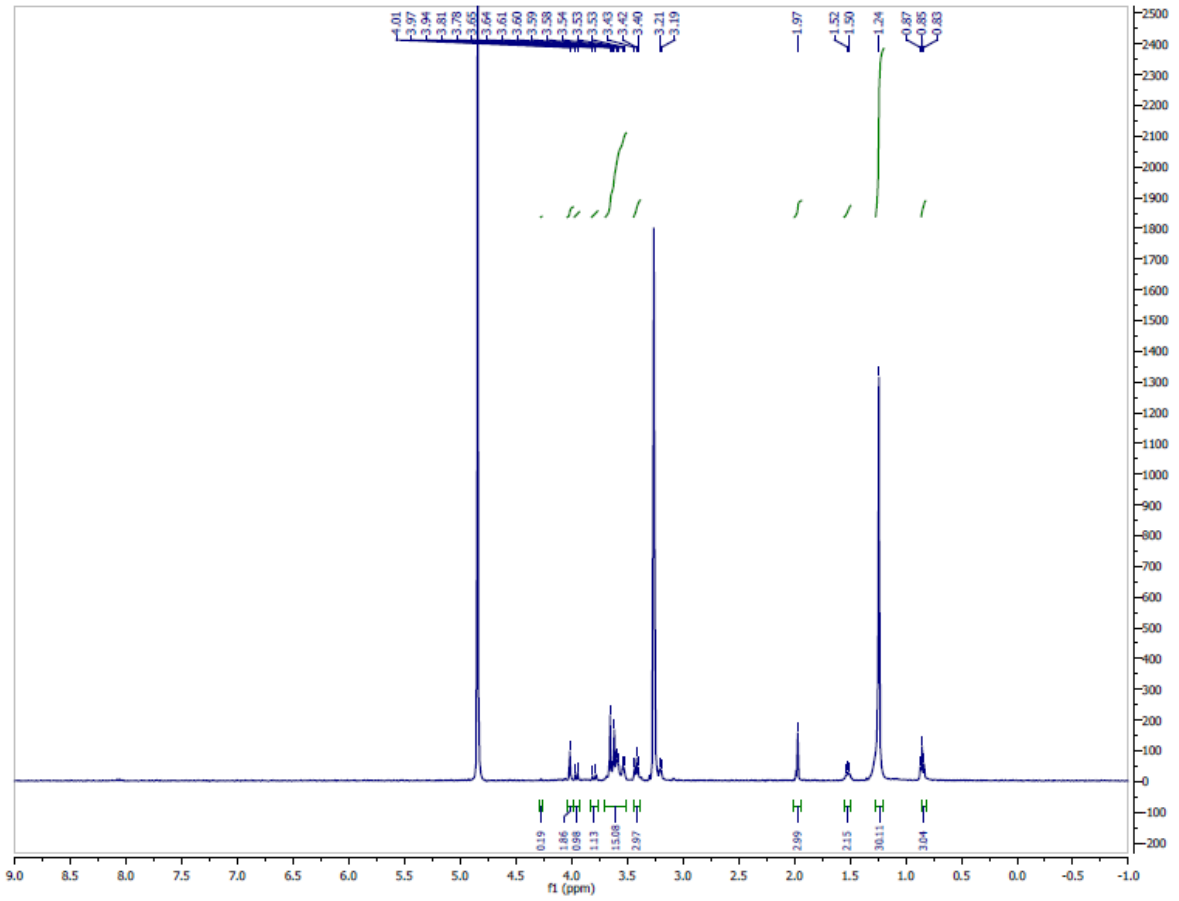

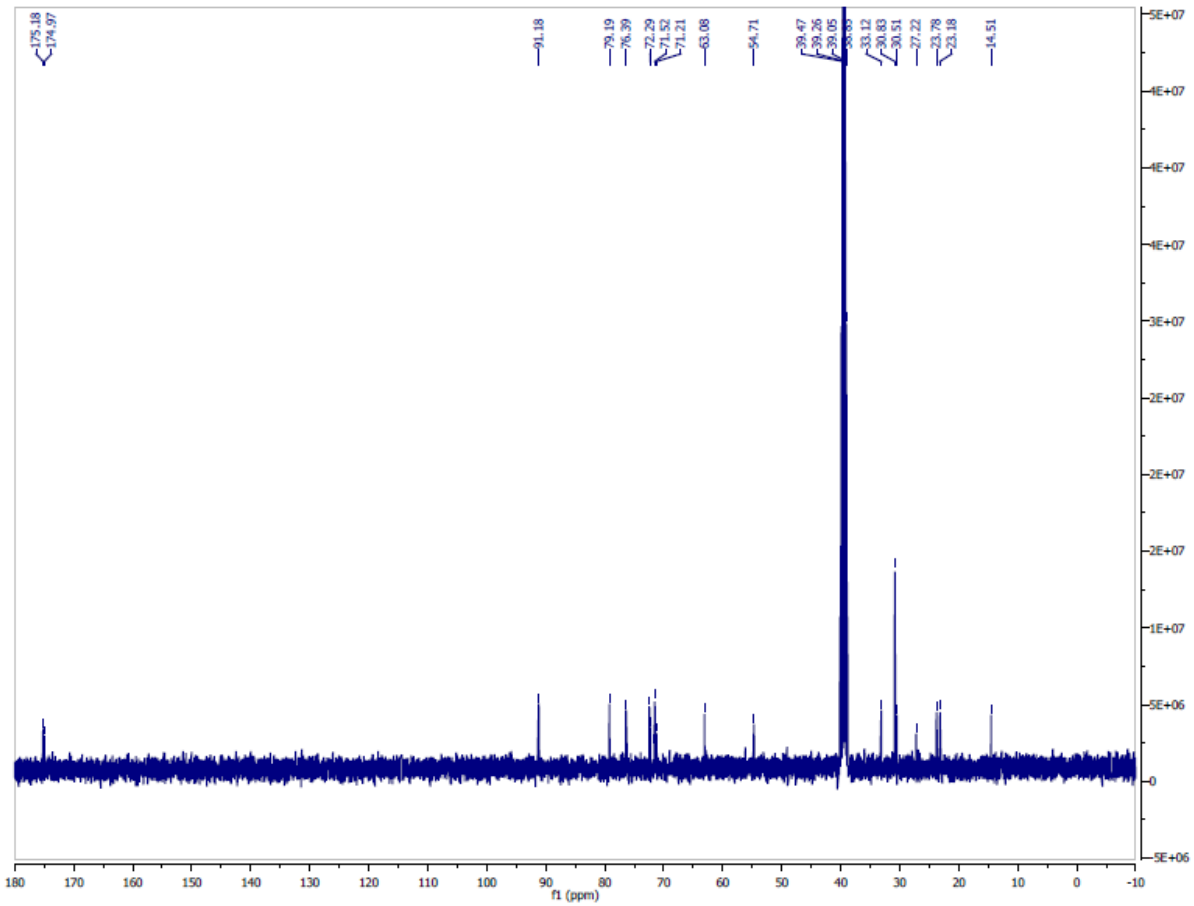

N’-(4-O-(β-Galactosyl)-1-deoxyglucopyranos-1-yl)-3,6,9,12-tetraoxatriacontanehydrazide **2c**

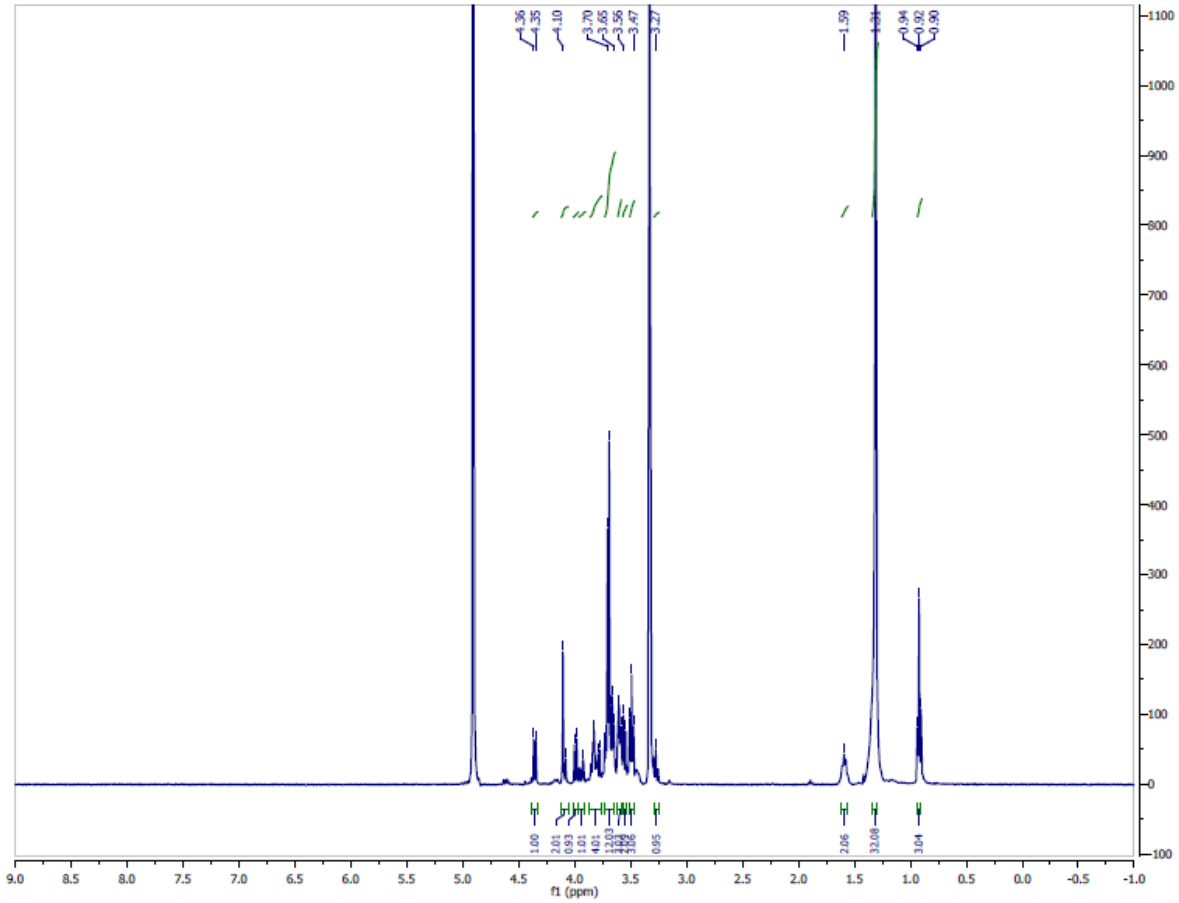

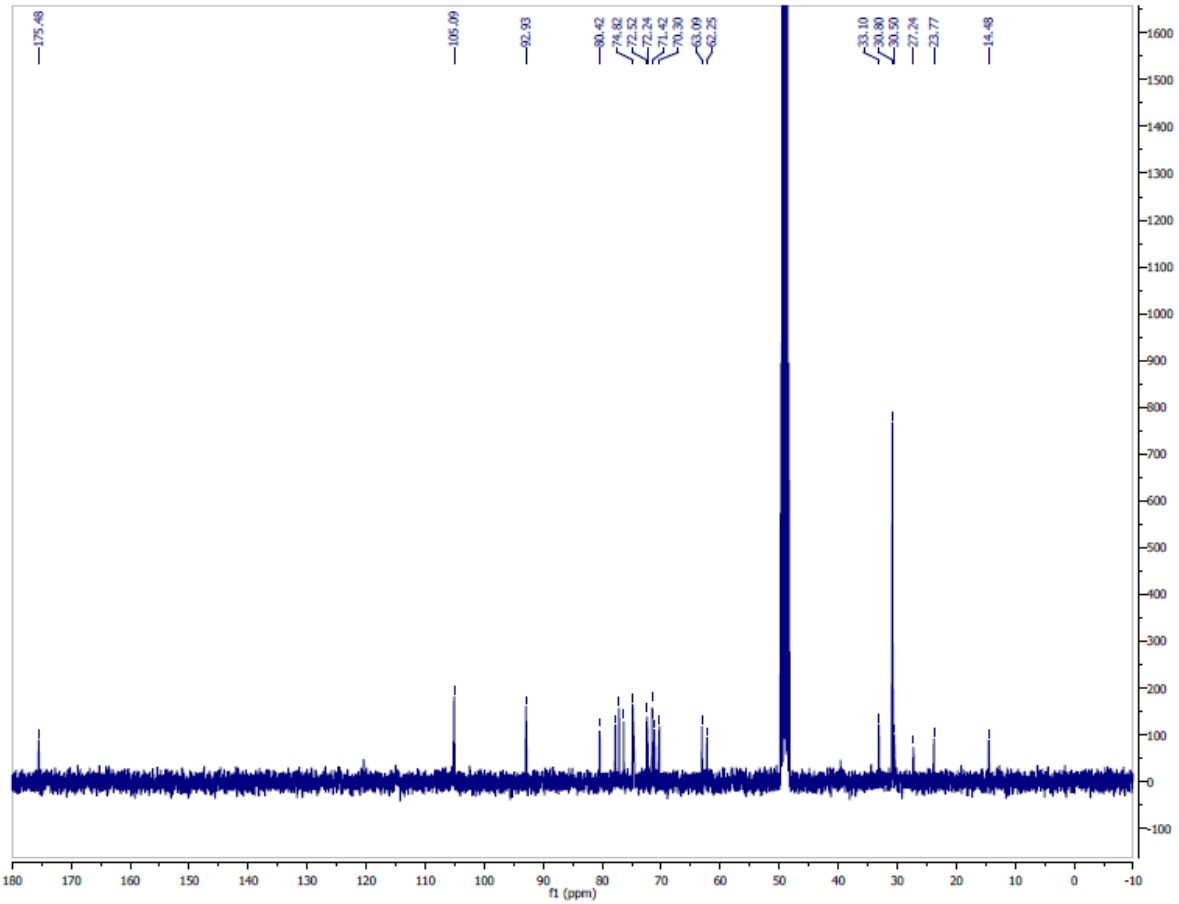

5-(2-(3,5-Dihydroxybenzoyl)hydrazine-1-carbothioamido)-fluorescein **4**

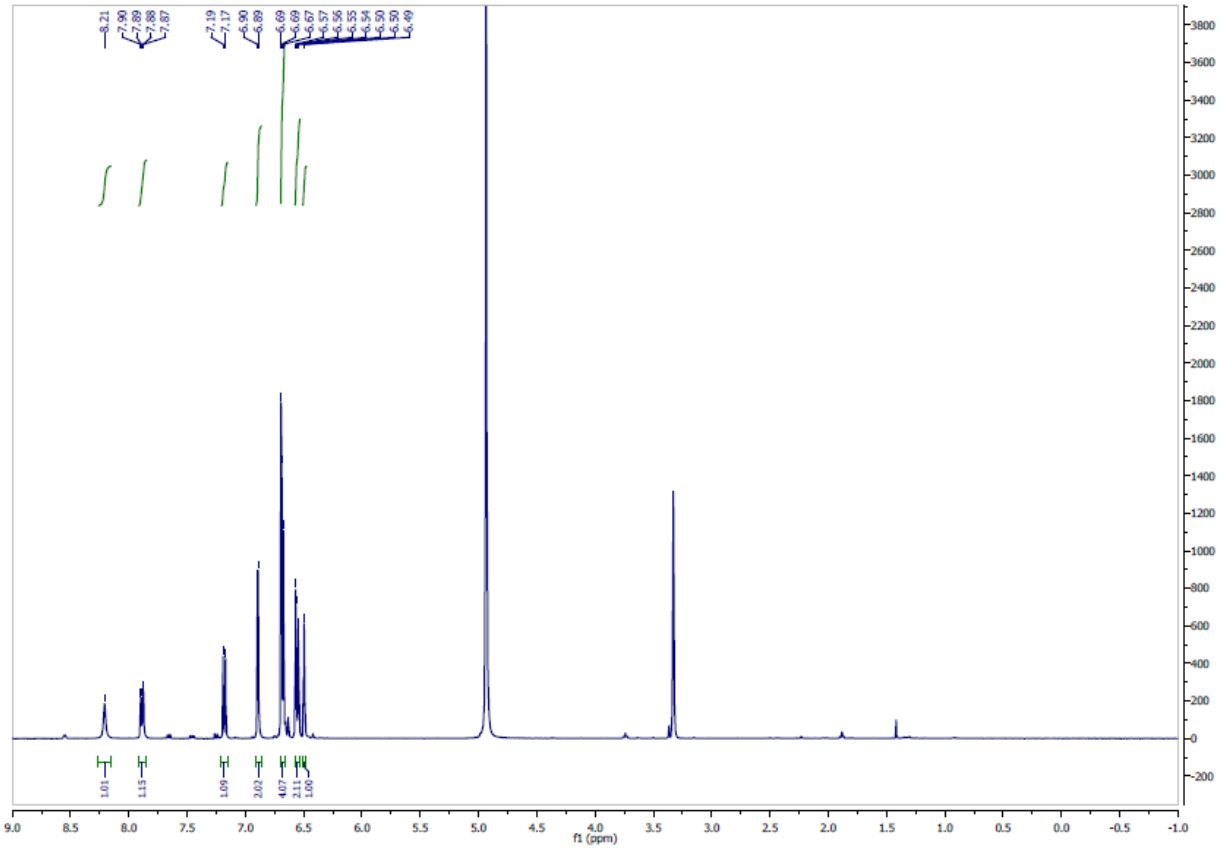

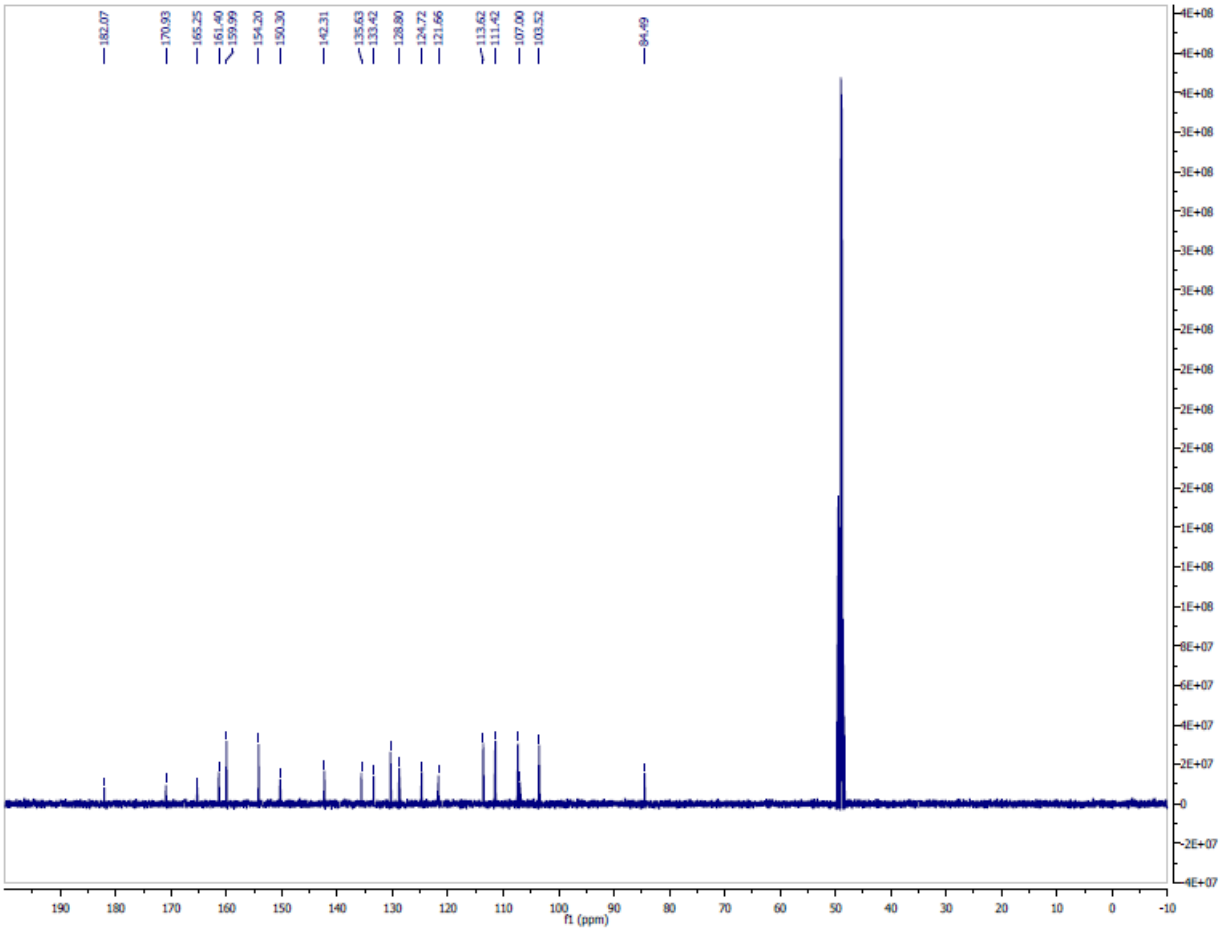

5-(2-(3,4-Dihydroxybenzoyl)hydrazine-1-carbothioamido)-fluorescein **5**

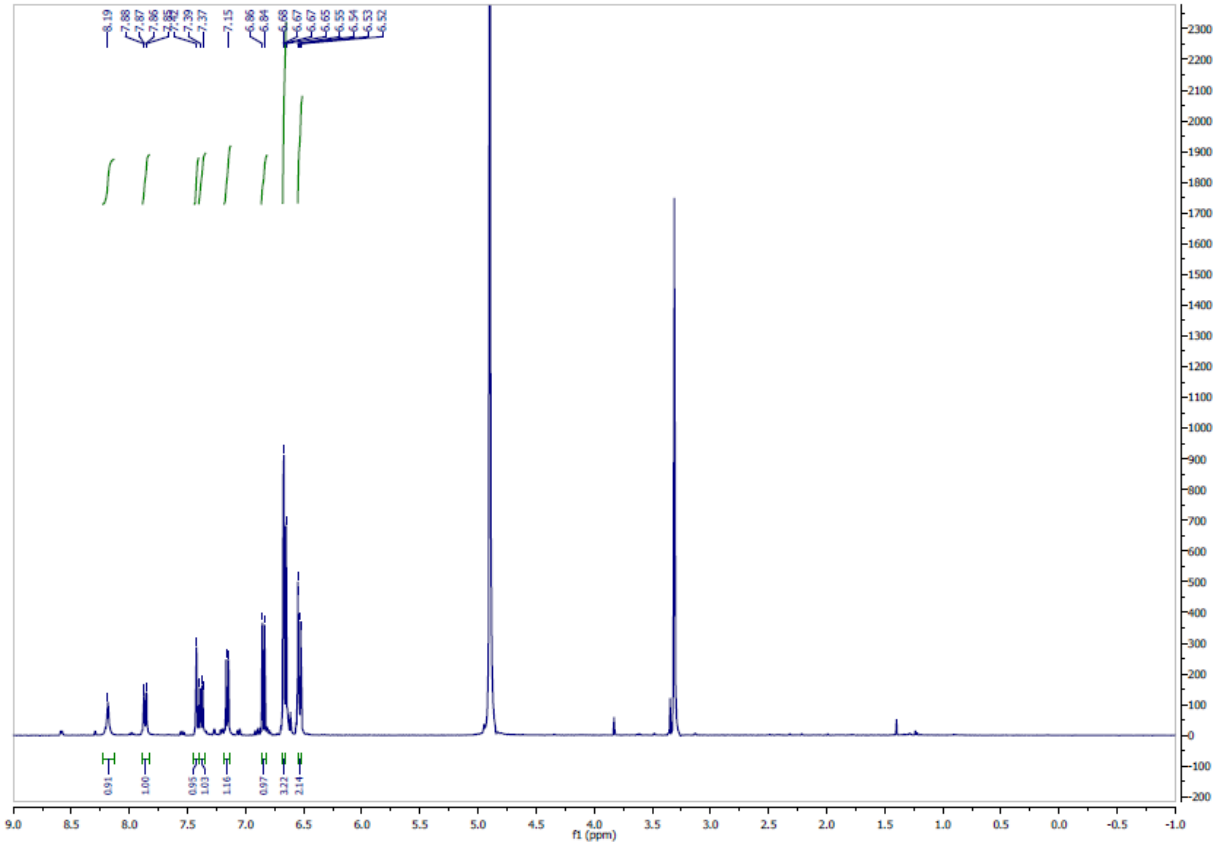

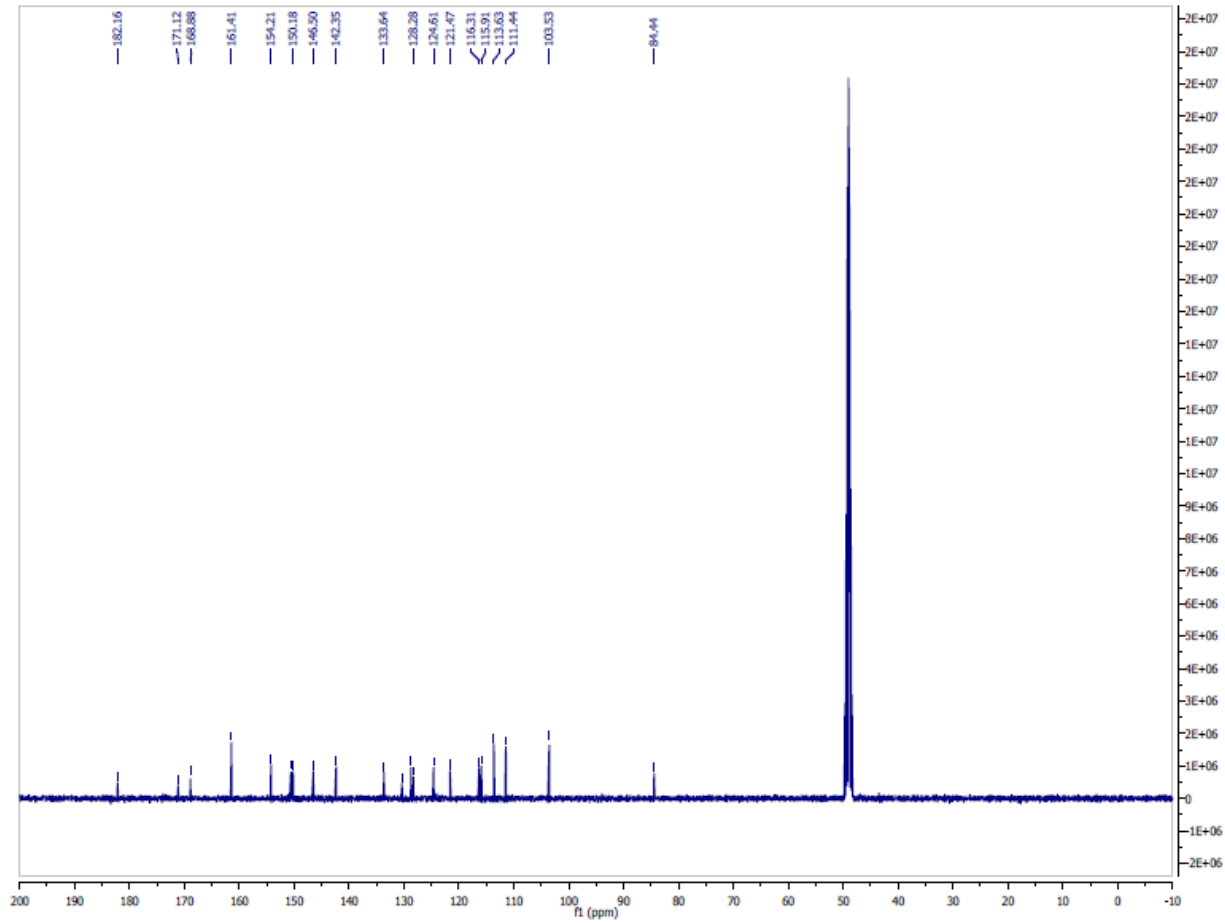

3,4-Dihydroxy-N’-(1-deoxyglucopyranos-1-yl)-benzohydrazide **3a**

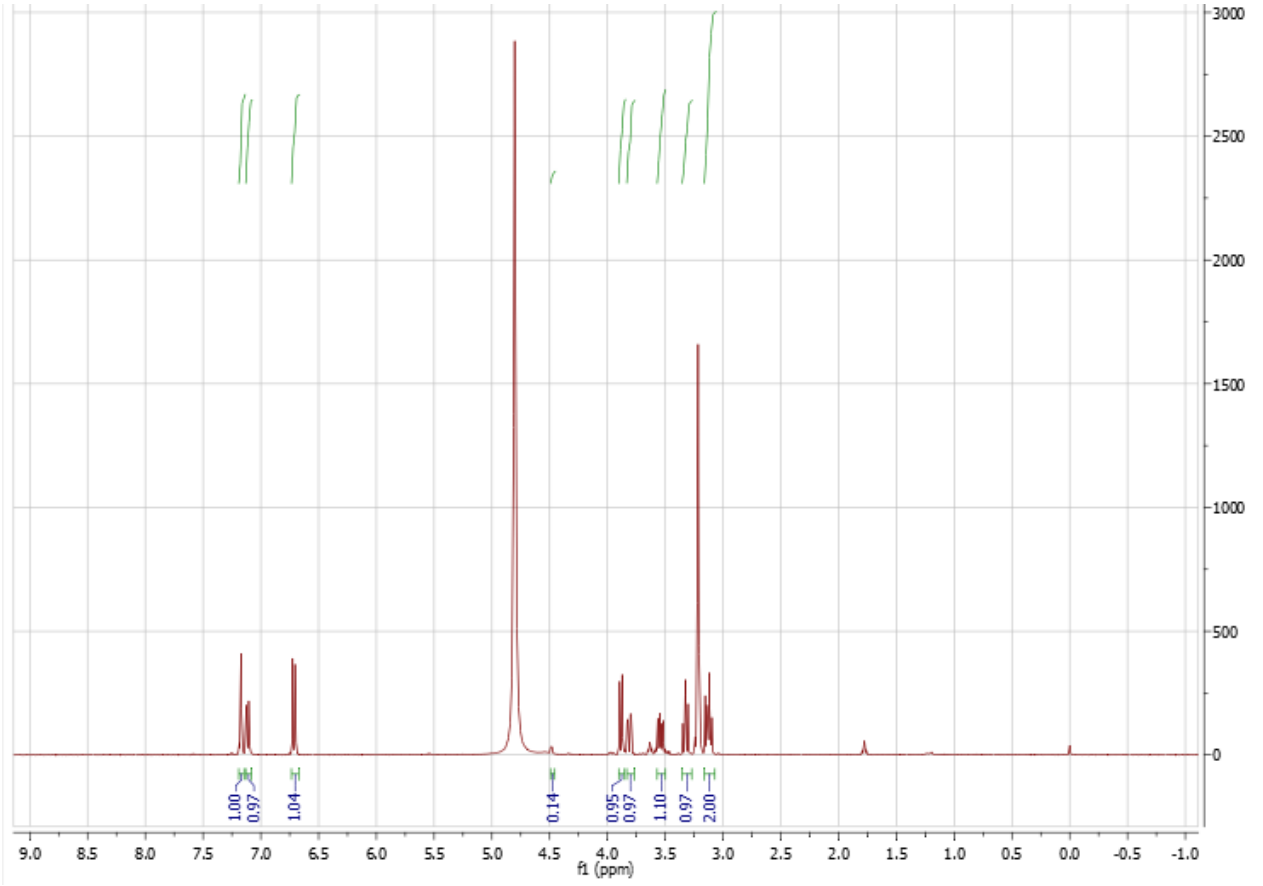

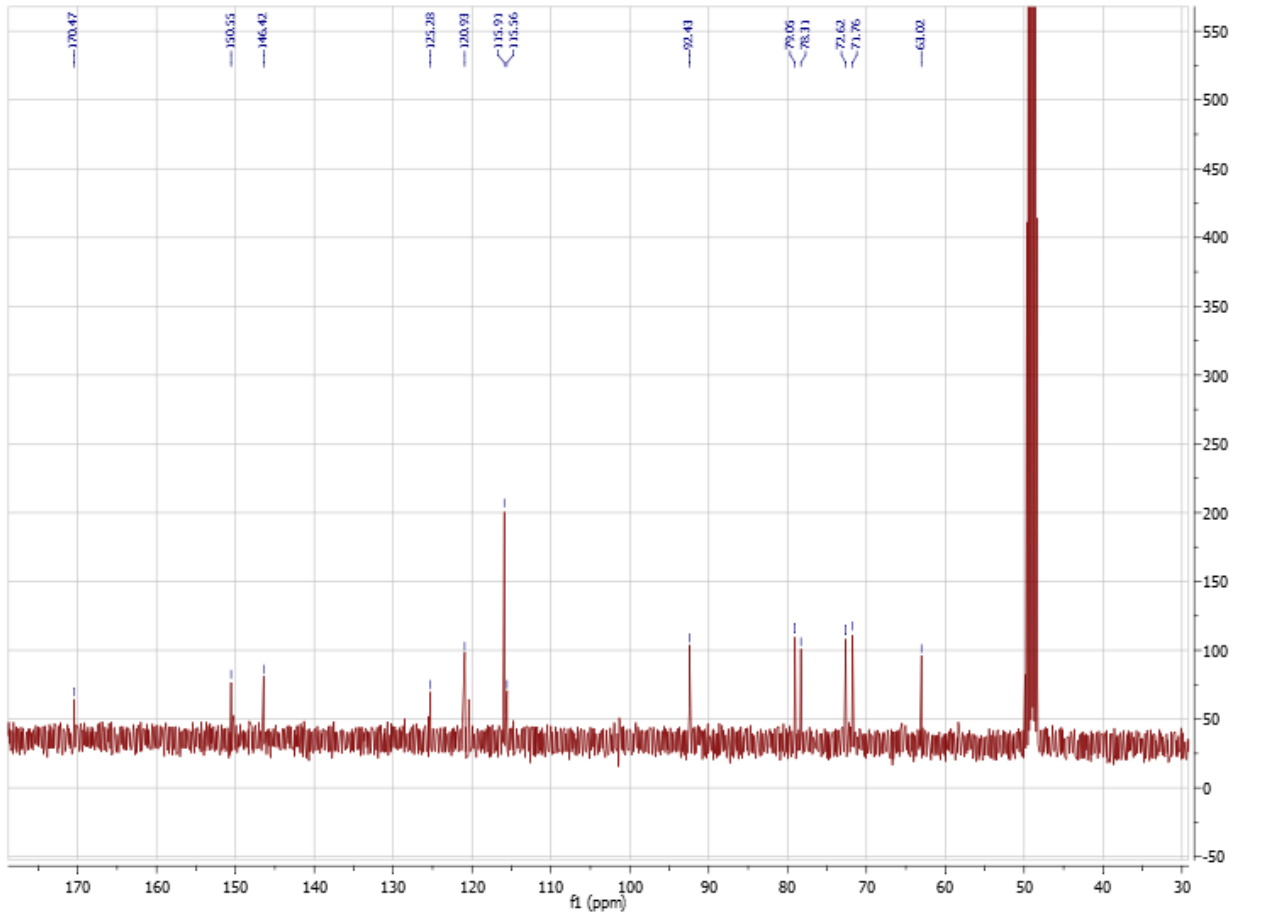

3,4-Dihydroxy-N’-(1,2-dideoxy-2-(acetylamino)-glucopyranos-1-yl)-benzohydrazide **3b**

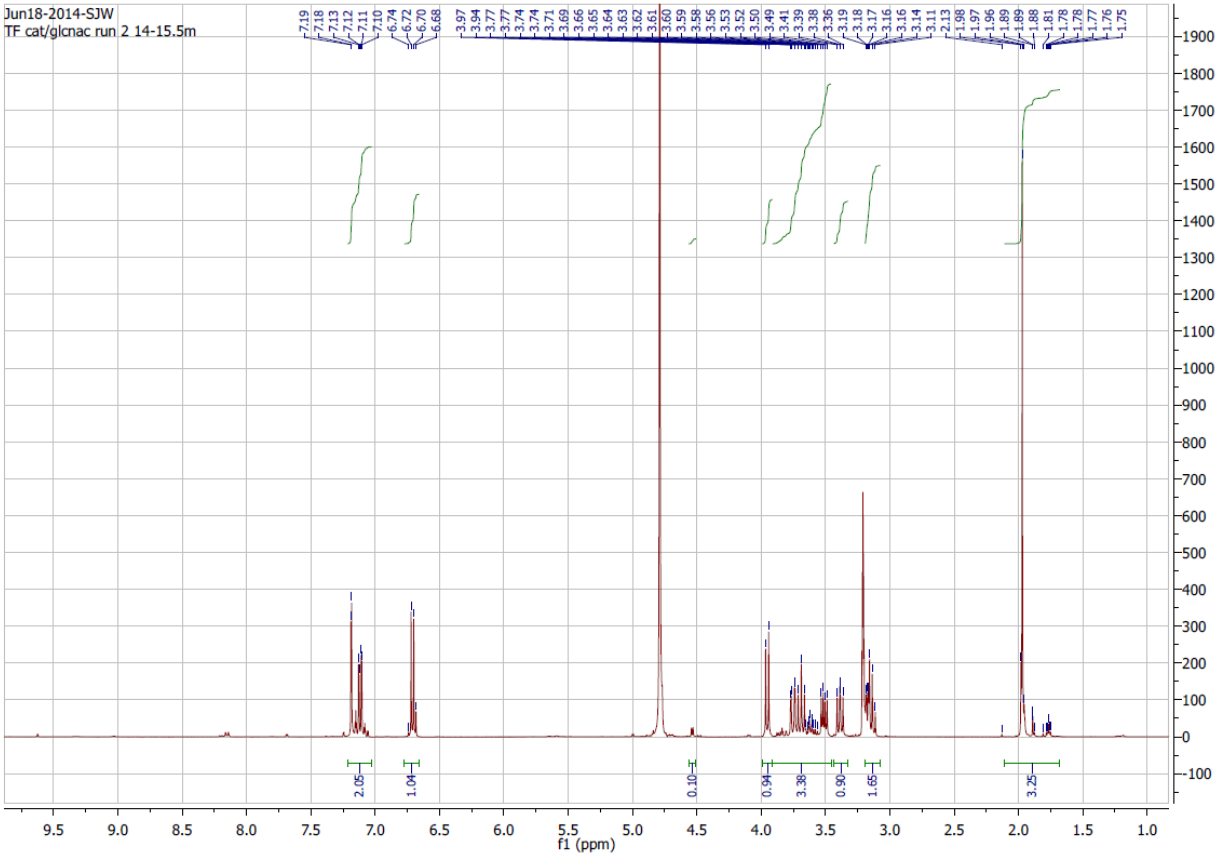

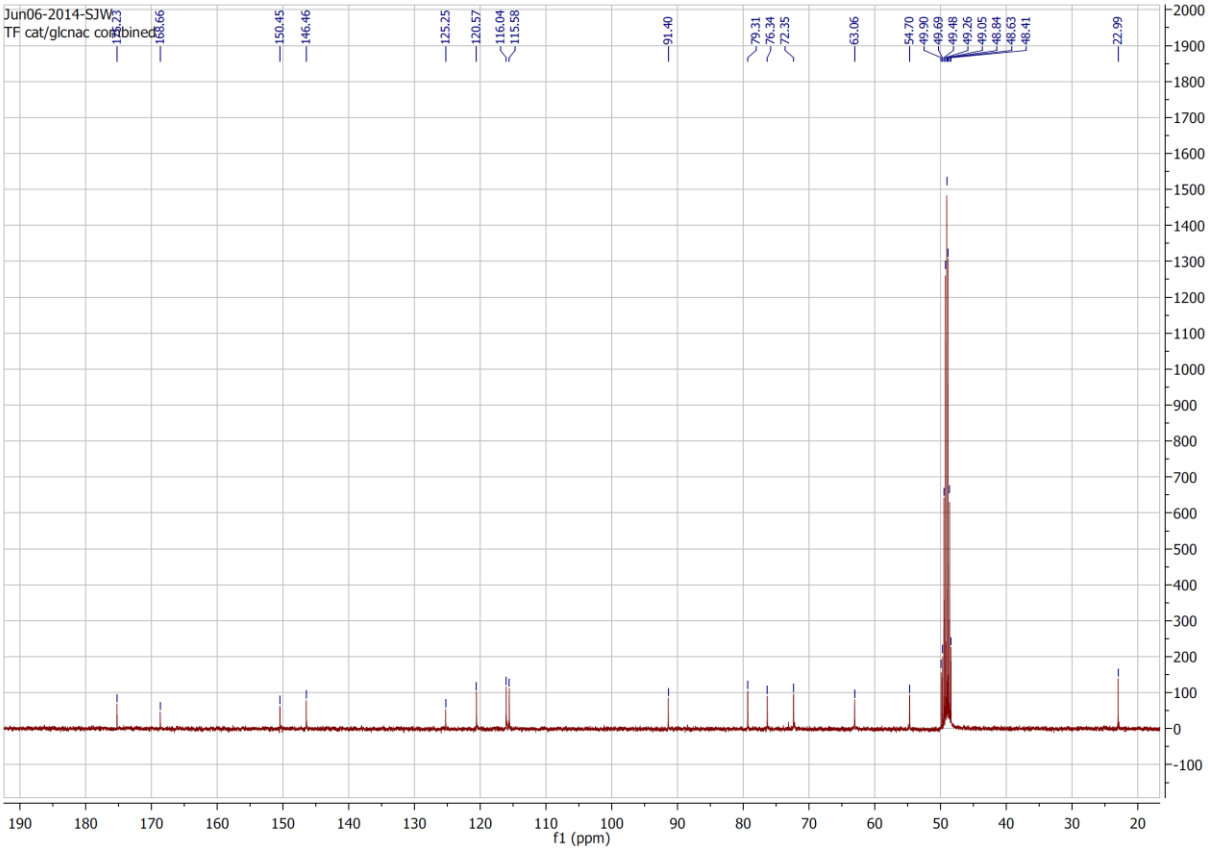

3,4-Dihydroxy-N’-(4-O-(β-galactosyl)-1-deoxyglucopyranos-1-yl)-benzohydrazide **3c**

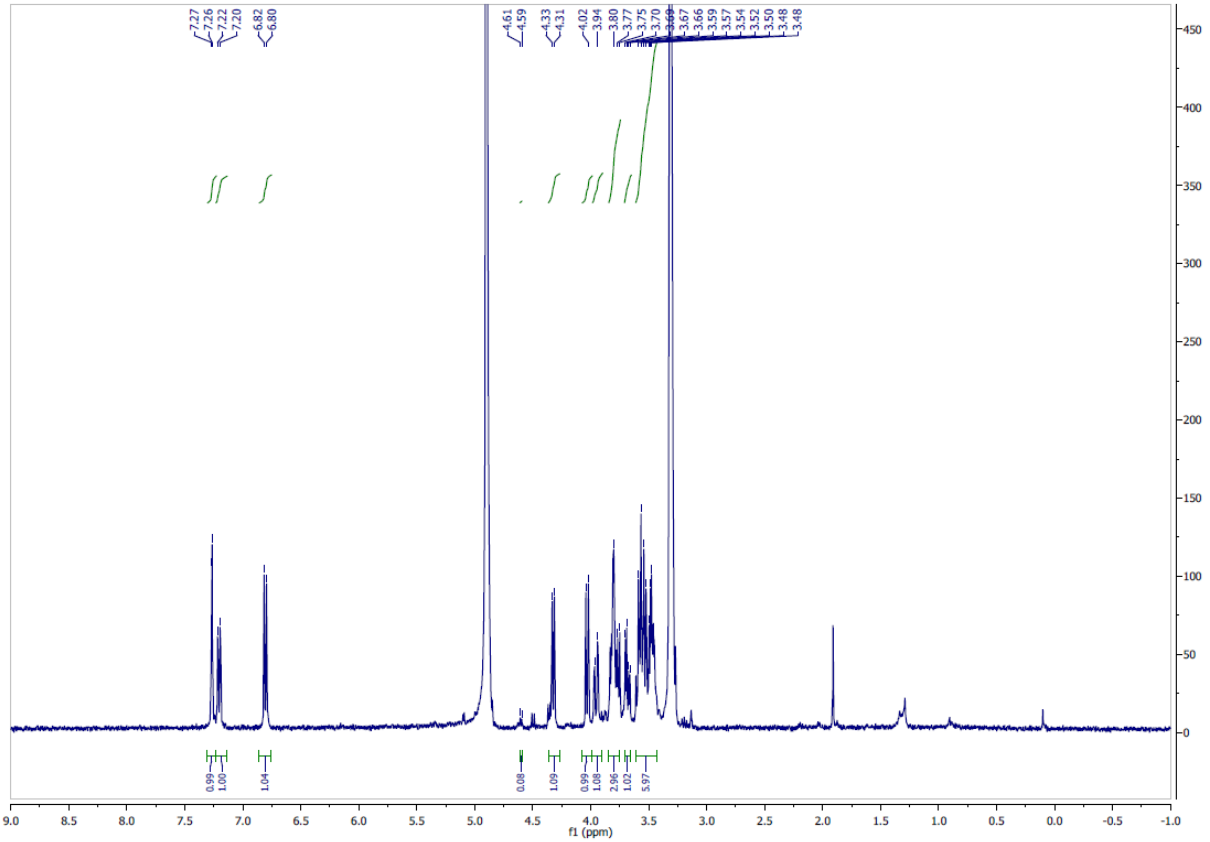

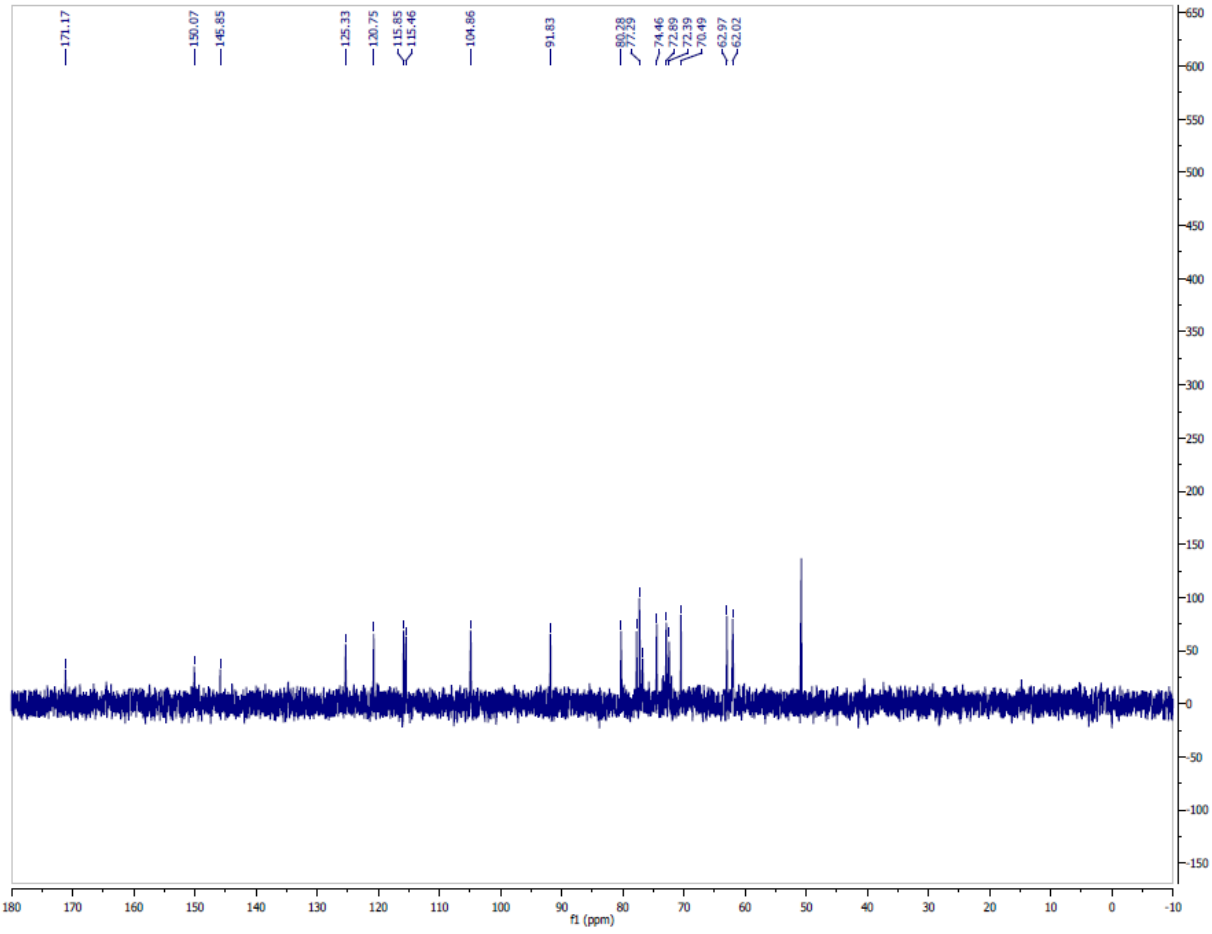

3,4-Dihydroxy-N’-(1-deoxy-4-O-(3-O-(N-acetyl-α-neuraminosyl)-β-galactopyranosyl)glucopyranos-1-yl)-benzohydrazide **3d**

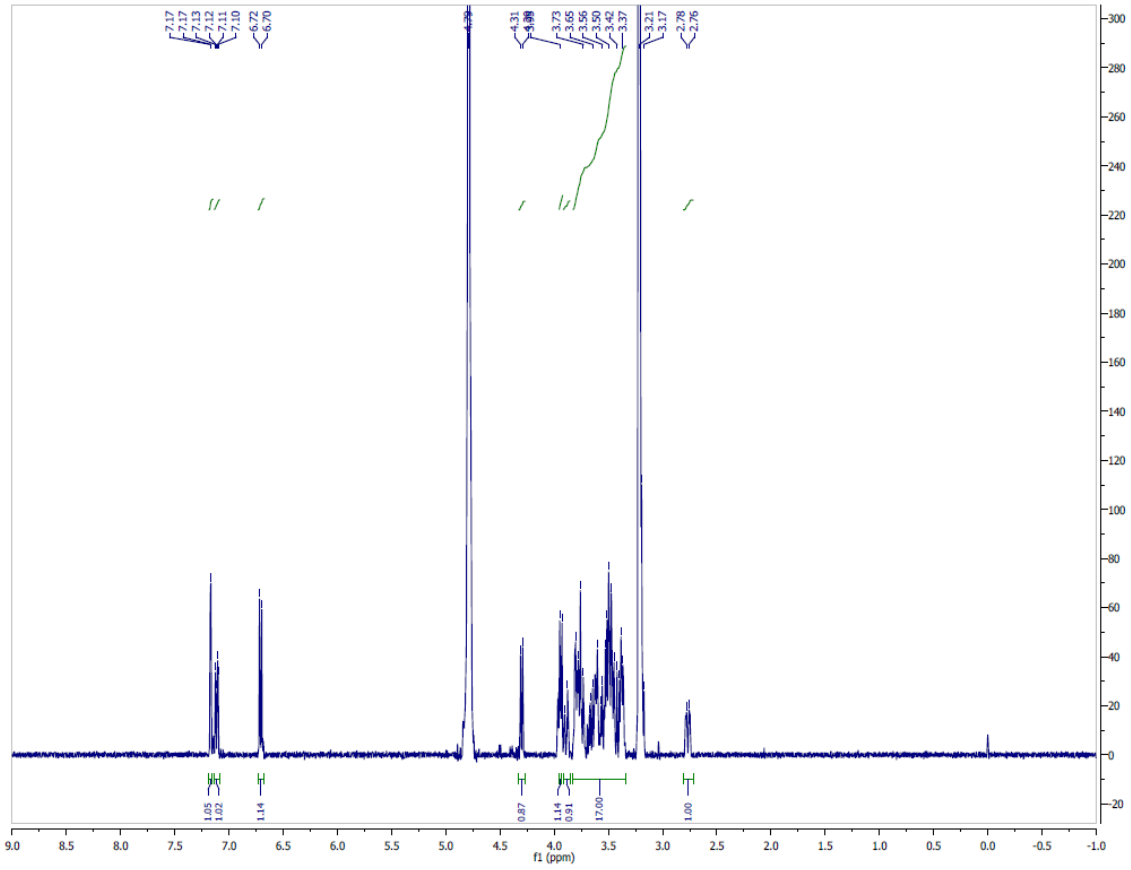

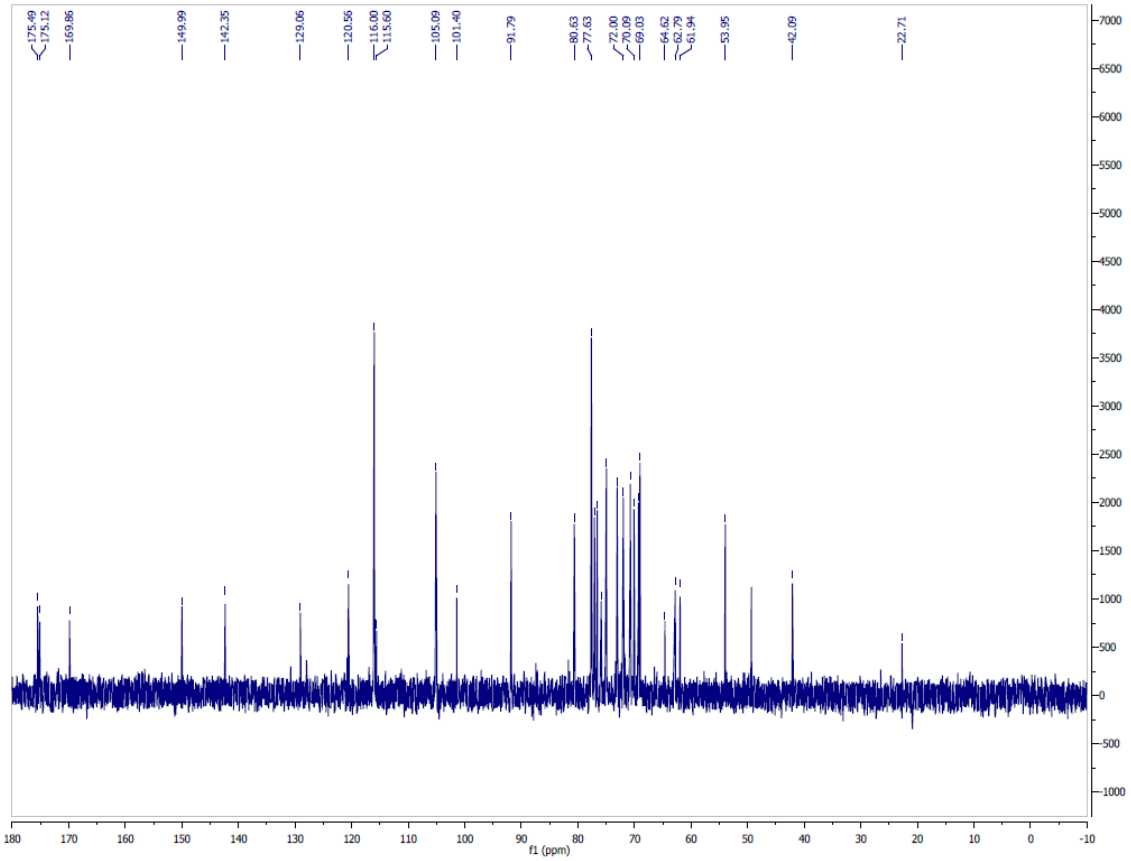

References

[1] M. A. Pilkington-Miksa, S. Sarkar, M. J. Writer, S. E. Barker, P. A. Shamlou, S. L. Hart, H. C. Hailes and A. B. Tabor, *Eur. J. Org. Chem*. 2008, 2900–2914

[2] B. Chen, U. Baumeister, G.Pelzl, M. K. Das, X. Zeng, G. Ungar, and C. Tschierske, *J. Am. Chem. Soc.*, 2005, **127**, 16578–16591

[3] T. Coxon, A. Almond, J. E. Gough and S. J. Webb, *MRS Proceedings*, 2014, **1688**, mrss14-1688-y08-13

[4] A. Booth, T. Coxon, J. E. Gough and S.J. Webb, *MRS Proceedings* 2014, **1688**, mrss14-1688-y05-14

[5] A. Streitwater Jr. and H. S. Klein, *J. Am. Chem. Soc.*, 1963, **85**, 2759-2763

[6] P. K. Glasoe and F. A. Long, *J. Phys. Chem.*, 1960, **64**, 188-189

[7] J. Kalia and R. T. Raines, *Angew. Chem. Int. Ed. Engl.*, 2008, **47**, 7523-7526

[8] B. Seantier, C. Breffa, O. Félix and G. Decher, *J. Phys. Chem. B*, 2005, **109**, 21755-21765